# A DEVICE FOR EXPERIMENTAL OBSERVATION OF FLUX VORTICES TRAPPED IN SUPERCONDUCTING THIN FILMS

by

Francis Patrick Rogers

Submitted to the

**DEPARTMENT OF ELECTRICAL ENGINEERING AND COMPUTER SCIENCE**

in partial fulfillment of the requirements for the degrees of

**BACHELOR OF SCIENCE**

and

**MASTER OF SCIENCE**

at the

**MASSACHUSETTS INSTITUTE OF TECHNOLOGY**

September 1983



Signature Redacted

Signature of Author _____
Department of Electrical Engineering and Computer Science, August 5, 1983

Signature Redacted

Certified by _____
Professor Terry P. Orlando, Thesis Supervisor

Signature Redacted

Certified by _____
Dr. Stuart Bermon, Company Supervisor, I.B.M. Research Division

Signature Redacted

Accepted by _____
Professor Arthur C. Smith, Chairman, Departmental Committee on Graduate Students

# A DEVICE FOR EXPERIMENTAL OBSERVATION OF FLUX VORTICES TRAPPED IN SUPERCONDUCTING THIN FILMS

by

Francis Patrick Rogers

Submitted to the Department of Electrical Engineering and Computer Science on July 25, 1983 in partial fulfillment of the requirements for the Degree of Master of Science in Electrical Engineering

## ABSTRACT

This experimental study developed a device for examining individual flux vortices in Type II superconducting thin-films. Using a precision X-Y positioning slide assembly at 4.2 $^{\circ}K$, this device can scan a 1/4" square chip locating incidences of trapped vortices. An rf-SQUID serves as the flux magnetometer, detecting the presence of these vortices with a typical signal-to-noise of 5:1. The scanning resolution was 0.020 inches.

Automated chip scans are possible due to a digital motor-controller. This makes the device expecially appropriate for large data-gathering experiments. The motor-controller sweeps the magnetometer sense-coil in a raster pattern over the entire chip surface, recording the occurrence of flux vortices on an analog X-Y Plotter.

This thesis also discusses the ferromagnetic shielding system used to provide a low-field environment for operation of this sensitive device. Field gradients were reduced to less than 10 $\mu G$ per inch. The field stability was better than 0.5 $\mu G$ per day. The uncompensated, absolute field perpendicular to the plane of the chip was $\cong$ 130 $\mu G$, but was nulled to several microgauss.

Lastly, results of scans across a perforated film are shown. Single, as well as double, occupation of vortex-attractive holes in a Niobium thin-film were observed.

Thesis Supervisor: Professor Terry P. Orlando, M.I.T. Department of Electrical Engineering

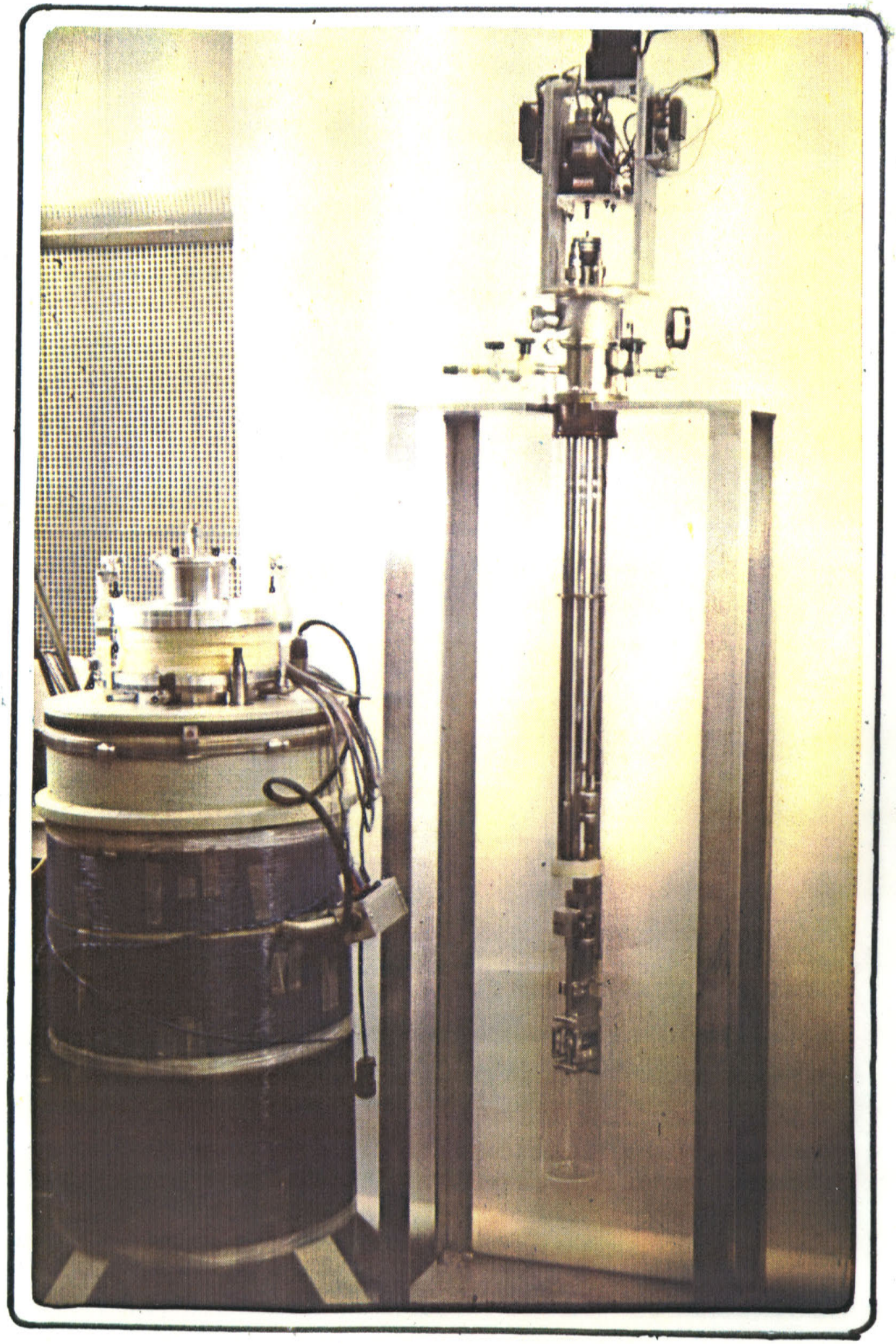

FIGURE 1

# ACKNOWLEDGEMENTS

I am most grateful to Stuart Bermon for coming up with the idea of a flux scanner and sharing it with me. Throughout the whole time I worked on the flux scanner, Stu was always attentive to my concerns and available for much-appreciated advice. His contribution to this thesis cannot be underestimated. In the lab, John Smith and Lou Gulitz were my biggest help. If they weren't lending me their tools or giving me some of their time-proven lab expertise, they were providing me with friendship and encouragement.

I want to thank my thesis advisor at M.I.T., Professor Terry Orlando, for his interest in the idea of a flux scanner. He always made time to talk to me whenever I sought him out. He also read my thesis from cover to cover, correcting my mistakes. I deeply appreciate anyone who takes the time to do this. John Tucker, head of the VI-A Program, is another M.I.T. person who takes a sincere interest in his students. He makes every effort to understand their viewpoint and answer their needs as best as one possibly could.

I appreciate the constant interest in the flux scanner project shown by Mark Ketchen and Walter Henkels, my two I.B.M. managers. They were my best source of positive feedback. In the machine shop, where I spent a significant portion of my time, the men behind the input desk were invaluable as well. Bob Jackson, Earl Fulsom, and Frank Franco sped my designs through the shop floor and often gave me special consideration. I finally want to thank all the members of the Josephson Project for their miscellaneous favors and friendliness. I scavenged many of their labs for sincerely appreciated equipment and spare parts.

I also want to mention the names of Bill Gallagher and Ephraim Flint. During my first assignment at I.B.M., Bill gave me the nicest possible introduction to the Research Center that one could possibly hope for. He set a highly favorable tone which was to endure for the next three summers I spent there. Eph entertained me on the weekends by teaching me how to sail. I never would have made it through the period I worked on my thesis if he hadn't shared his passion for sailing with me.

Lastly, I'm grateful to the I.B.M. Corporation for becoming a member of the M.I.T. Co-op Program, and supporting several new students each year. Working at the Research Center is a valuable education in itself.

# BIOGRAPHICAL NOTE

Francis Patrick Rogers was born in Seattle, Washington on Sept. 18, 1960. For high school, he attended Matteo Ricci College which included three years at the old Seattle Preparatory School and one year at Seattle University. He entered the Massachusetts Institute of Technology in Sept. 1978, subsequently majoring in Electrical Engineering with a concentration in Political Science. While an undergraduate, he was admitted into the Electrical Engineering Co-op Program with the International Business Machines Corporation as his sponsor company. For two summers he worked at I.B.M.'s Thomas J. Watson Research Center located in Yorktown Heights, New York. In Jan. 1982, the Department of Electrical Engineering and Computer Science accepted him into the graduate degree program. He entered with the intention of completing the research for his Master's Thesis at I.B.M. in the Josephson Technology group. He worked full time at I.B.M. from June 1982 through Jan. 1983, completing all the experimental work. The thesis was actually written and completed during the summer of 1983.

The author is a member of: Eta Kappa Nu, the honorary electrical engineering society; Tau Beta Pi, the honorary engineering society; and an associate member of Sigma Xi, the scientific research association. As an undergraduate, he rowed for the freshman lightweight crew team, and earned a varsity letter in Alpine Skiing. He was elected president of Phi Delta Theta Fraternity for one term.

To my parents-- Jane Bergstrom Rogers and Francis Patrick Rogers

and to my brothers-- John Bergstrom Rogers, Christopher Thor Rogers,
Eric Joseph Rogers, and Wilfrid Rogers

# TABLE OF CONTENTS

4. OBSERVATION OF TRAPPED VORTICES IN THIN FILMS



5. CONCLUSION

# CHAPTER I: INTRODUCTION

The objective of this thesis was to build a device which would enable the direct observation of trapped vortices of magnetic flux in superconducting thin films. We named this device the "flux scanner" for the reason that it would scan a thin film, recording the flux density emanating from the film, versus position. Sharp peaks of concentrated flux would reveal the presence of individual vortices. One of the critical motivations for building the flux scanner was the anticipated cheapness and ease of conducting experiments once the device was complete. S. Bermon had previously designed on-chip Josephson interferometers to detect trapped flux located in holes in the chip's superconducting ground plane[1]. This method involved a long turn-around time for chip fabrication, as well as, considerably expense. It was recognized that the flux scanner would speed up experimentation at a greatly reduced cost.

Work on the flux scanner began in June of 1980. Joel Fajans&2, under the direction of Stuart Bermon of I.B.M. Research, designed the original mechanical and electrical equipment. In January of 1980, I took up where Joel left off. Since that time, I've spent a total of 14 months working full-time on this project in cooperation with Stuart Bermon. With the completion of this thesis, the flux scanner is basically operational. It can observe individual flux quanta with a high degree of reproducibility. The mechanical scanning operation has yet some difficulties to be overcome before reliable operation is ensured though. Fortunately, we have the advantage that most of the problems are well-understood, and with a few additional refinements, this device will hopefully be used in the future for a wide range of data-gathering experiments. Some possible candidates are:

(1) analyzing magnetic field plots to determine the characteristic flux distribution of a single vortex trapped in a film inhomogeneity.

(2) experimentally determining the probability of vortices being trapped in small holes etched through a thin film, rather than being trapped in intrinsic film defects. These holes represent potential energy wells with a characteristic vortex attraction energy.

(3) experimentally determining the relative probability of trapping flux in holes of different size and shape.

(4) observing the movement of vortices in the film from inhomogeneity to inhomogeneity under the influence of a current density exerting a force,

$$F = \int_{V_{film}} \vec{J}_{film} \times \vec{H}_{vortex} dV_{film}$$

This report describes the flux scanner experiment in five chapters. Chapter I is this introduction. Chapter II covers the theory of flux vortices pertinent to understanding the operation of the flux scanner. It discusses the far-field appearance of vortices, as well as, the trapping energies associated with holes in thin films. Chapter III provides a detailed description of the flux scanner. It discusses the mechanical and electrical scanning equipment, along with the flux magnetometer and magnetic shielding which was necessary to "see" the vortices. Chapter IV takes a look at the experimental results discussing several chip scans in detail. Finally, Chapter V concludes with a description of future improvements which are necessary to fulfill the goal of reliable operation of the flux scanner.

## NOTES

1. S. Bermon and T. Gheewala, Moat-Guarded Josephson SQUIDS, presented at the Applied Superconductivity Conference (1982).

2. Present Address: Massachusetts Institute of Technology, Department of Electrical Engineering and Computer Science, Room 38-444, 77 Massachusetts Avenue, Cambridge, Massachusetts 02139.

# CHAPTER II: THEORETICAL BACKGROUND

## FLUX TRAPPING IN TYPE II SUPERCONDUCTORS

The presence of discrete bundles of magnetic flux penetrating through the interior of a sample characterizes Type II superconductors. Above a certain critical value $H_{c1}$ of an applied field, long cylindrical threads of flux in the direction of the ambient field will begin to populate the superconducting bulk. At the higher critical value $H_{c2}$, enough flux will penetrate the sample so as to turn it completely normal with a continuous instead of quantized flux distribution throughout its bulk. Quantized flux penetration in Type II superconductors can however occur at fields well below $H_{c1}$, that is, if the Type II superconductor has localized crystalline defects or impurities which act as trapping sites, and if it is cooled through $T_c$ in the presence of an incident field. In the case of a Type II thin-film, flux trapping perpendicular to the plane of the film is also enhanced by the fact that the film thickness $d$ is much smaller than the planar dimensions of the film. It is more energetically favorable for the film to allow discrete flux filaments to penetrate, rather than exclude the flux, as the Meissner effect dictates for a bulk Type II superconductor, and suffer an appreciable loss in superconducting condensation energy $E_c$.

$$E_c = \int_V \frac{H_c^2}{8\pi} dV$$

(where $V$ is the volume of the superconductor.) The screening energy $E_s$ required to exclude all flux normal to the plane of the film directly subtracts from $E_c$ when calculating the total energy of the superconducting state relative to the normal state of a metal.

$$E_s = \int_{V'} \frac{H_s^2}{8\pi} dV' + E_{kin}$$

(where $H_s$ is the equivalent screening field produced by a superconductor to cancel the impinging ambient field in the region of the superconductor; $V'$ represents all space; $E_{kin}$ is the kinetic energy of the circulating currents in the superconductor necessary to produce the screening field.) In the case of a thin film attempting to totally exclude all flux from its interior, the screening energy is distributed over a relatively small superconducting volume (lower $E_c$) as compared to the large volume (higher $E_c$) of a bulk superconductor with similar surface area facing normal to the ambient field. Thus, to preserve the low-energy superconducting state, thin films allow quantized flux filaments to penetrate their interiors at fields well below $H_{c1}$. Hence, a thin film exhibits enhanced "flux trapping". On the following page is a simple diagram of the field lines surrounding a trapped fluxoid in a thin-film.

## FAR-FIELD APPEARANCE OF FLUX VORTICES IN THIN FILMS

J. Pearl[1] first found an analytical solution describing the structure of these flux filaments or "flux vortices" in thin films of Type II superconductors. He solved the Ginzburg-Landau equations assuming a superconducting order parameter of the form

$$\Psi = \Psi_0 e^{i\gamma} \qquad \text{where} \quad \psi_0 = \frac{c}{e^* \lambda}\sqrt{\frac{m^*}{4\pi}}$$

$m^*$ and $e^*$ being the Cooper pair effective mass and effective charge respectively. This form of the order parameter is uniform throughout the superconducting region surrounding the normal core of the vortex, but also assumes the same uniformity inside the normal core where the density of superconducting electron pairs $n_s$ goes to zero.

Although this model gives simple and accurate expressions for the supercurrent density and magnetic flux density outside of the core, these expressions diverge in the area within the core. J. Clem[2] proposed a more comprehensive solution to the Ginzburg-Landau equations,

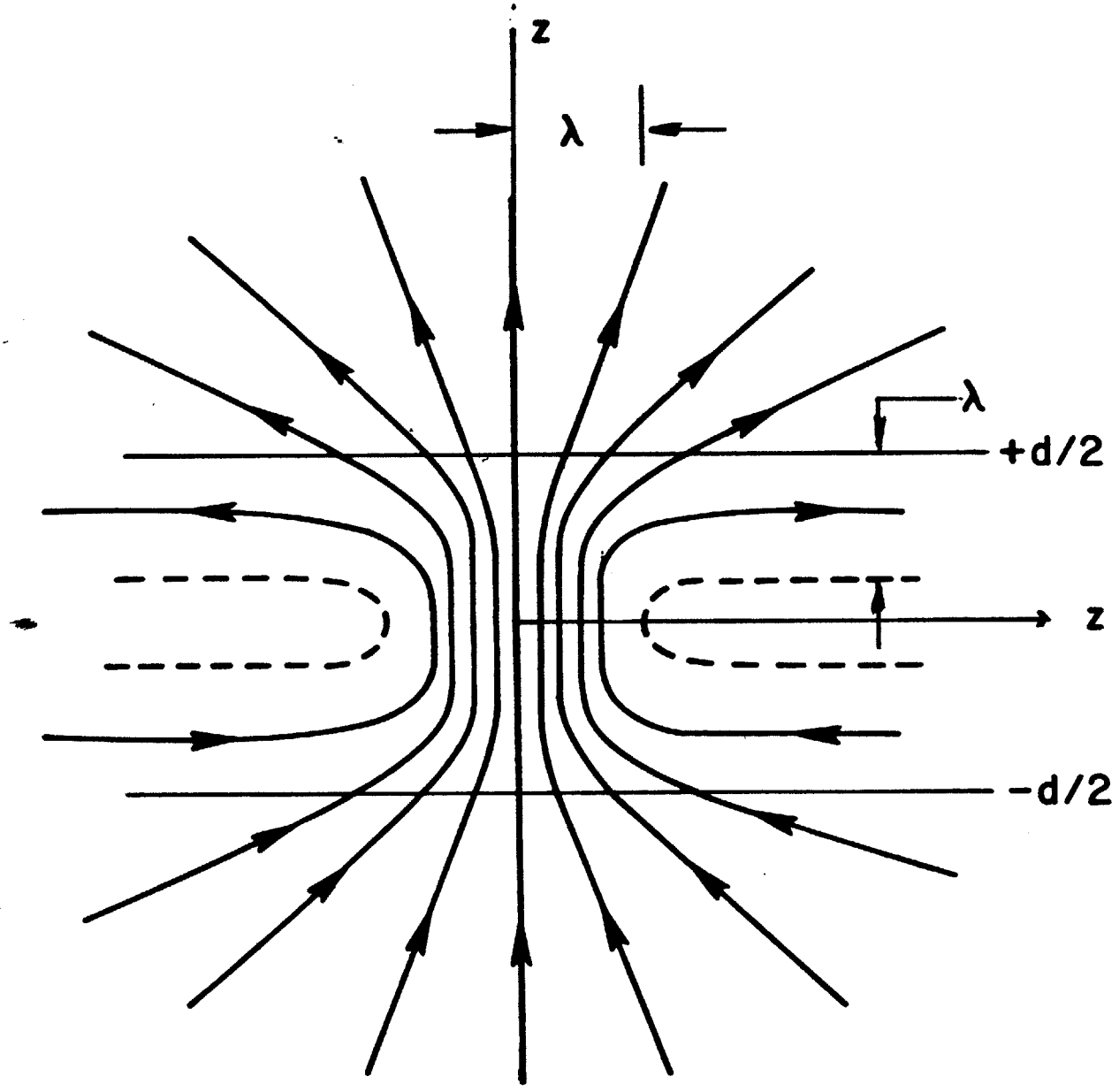


FIELD SURROUNDING FLUX VORTEX IN TYPE II THIN FILM OF THICKNESS d

FIGURE 2

assuming a variational trial function $f$ for the magnitude of the normalized order parameter where

$$f = \frac{\rho}{(\rho^2 + \xi_v^2)^{1/2}} \quad ( \Psi = f\Psi_o e^{i\gamma} )$$

The G-L equations reduce to the following expressions in which $a'$ is the vector potential:

$$\frac{1}{\kappa^2} \vec{\nabla}'^2 f + f (\vec{a}' + \frac{1}{\kappa} \vec{\nabla}' \gamma)^2 = f - f^3$$

$$\vec{\nabla}' \times (\vec{\nabla}' \times \vec{a}') = - f^2 (\vec{a}' + \frac{1}{\kappa} \vec{\nabla}' \gamma)$$

where the prime mark indicates a quantity's lack of dimension. For example, all distances are given in units of the penetration depth, $r' = r/\lambda$. In the same manner, the magnetic density is in units of $\sqrt{2}H_c$, the vector potential in units of $\sqrt{2}H_c\lambda$, and the energy density in units of $H_c^2/4\pi$.

These expressions can be solved analytically. Using this variational method, one arrives at expressions for the vector potential inside the bulk superconductor, at the vacuum-superconductor interface, and outside the superconductor. Then, by minimizing the free energy associated with this solution, one can arrive at values for $\xi_v$. It turns out that $\xi_v$ is dependent upon the Ginzberg-Landau parameter $\kappa$ ( $= \lambda/\xi$ ), the ratio of the penetration depth to the actual coherence length. For Type II superconductors, $1/\sqrt{2} \leq \kappa \leq \infty$, and in this range, $\xi_v/\xi$ varies with continously positive slope from *0.935* to *1.414*. On the following page is a graph of the resulting vortex structure for $\xi_v/\xi = 1.28$ ($\kappa \cong 5.13$)[3] Clem's analytical model closely approximates the numerical solution, and in addition, provides actual equations describing the structure of flux vortices both inside the normal core and outside of it as well.

In a later paper [4], and at a talk given at IBM in July of 1981, Clem described the variational thin-film vortex solution. The method of variational order parameters does not

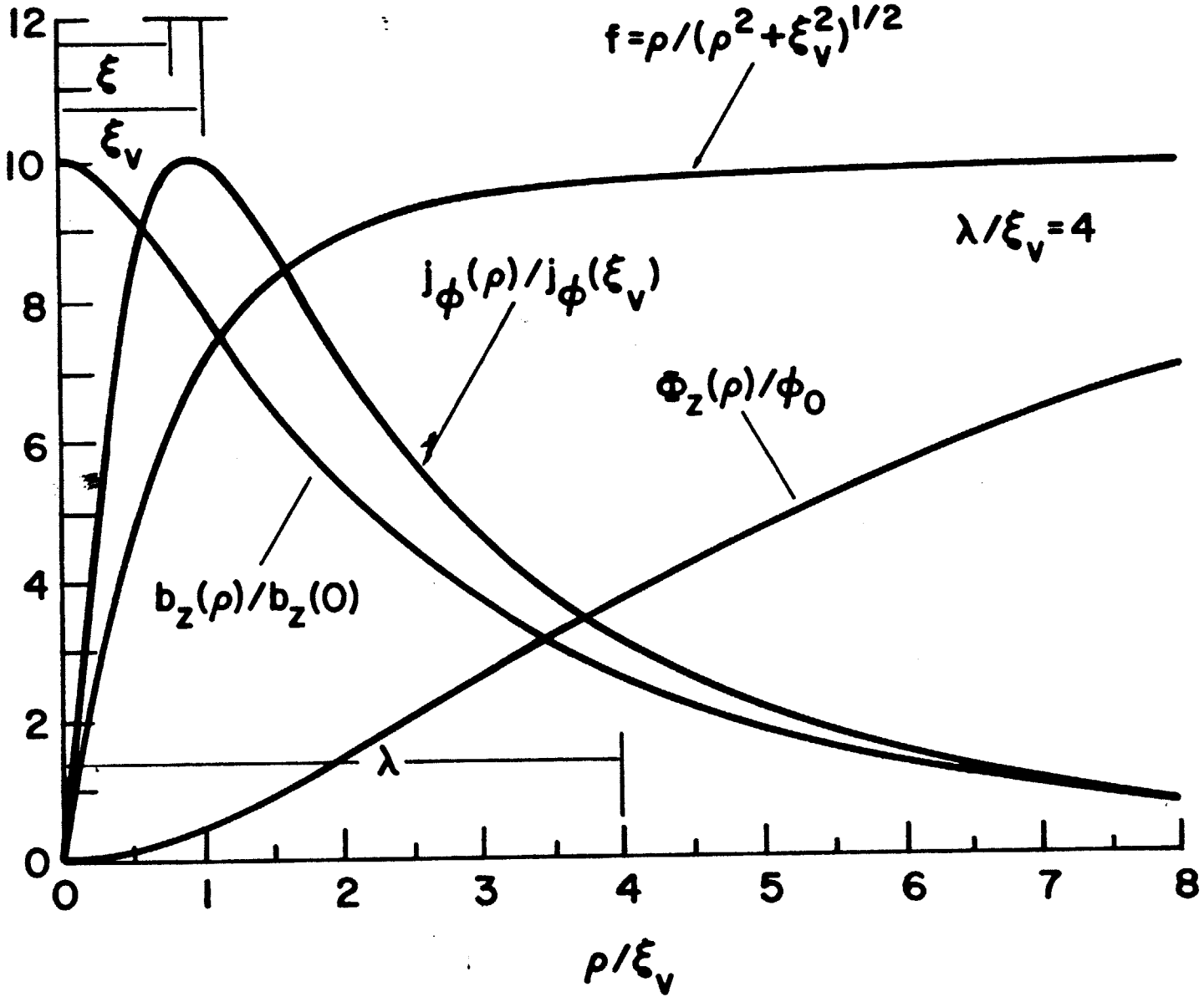


MODEL FOR VORTEX CORE IN TYPE II BULK SUPERCONDUCTOR ($\xi_v/\xi = 1.28$)

FIGURE 3

lead to an analytical solution in this case but does allow one to approximate the vortex field at distances much greater than $\lambda_{eff}$. Clem derived the following expression in cylindrical coordinates for the vector potential above the film $(z' > 0)$:

$$a'_{\phi}(\rho',z') = \frac{1}{\kappa}\int_0^{\infty} dq' \; f_1(q')f_2(q')f_4(q')J_1(q',\rho')e^{-q'z'}$$

where

$$f_1(q') = \frac{1}{1+q'^2} \qquad \text{(London Screening Function)}$$

$$f_2(q') = \frac{1}{1+\left(\frac{q'}{\sqrt{q'^2+1}}\right)\cot\left(\frac{d'\sqrt{q'^2+1}}{2}\right)} \qquad \text{(Film Geometry Function)}$$

$$f_4(q') = (1+q'^2)^{1/2}\frac{K_1\left(\xi'_v\sqrt{1+q'^2}\right)}{K_1}(\xi'_v) \qquad \text{(Core Cutoff Function)}$$

Both $J_1$ and $K_1$ are modified Bessel Functions.

Clem went on to derive the far-field approximation for a vortex which I will reproduce here. In the thin film limit $d'<<1$ $(d<<\lambda)$, all three functions $f_1$, $f_2$, and $f_3$ reach steady state finite values of approximately *0*, *1*, and *1* respectively within the distance

$$q' = \frac{2}{d'} = \lambda'_{eff} >> 1$$

Rearranging,

$$\lambda_{eff} = \frac{2\lambda^2}{d} \quad (= \lambda_{\perp})$$

Thus, outside of $\lambda_{eff}$, these three functions are well-behaved.

In the integral for $a_{\varphi}'(\rho',z')$, the expression

$$J_1(q',\rho')e^{-q'z'}$$

has a natural cutoff at

$$q' \cong \frac{1}{\sqrt{\rho'^2+z'^2}} = \frac{1}{r'}$$

where r is the radial component in spherical coordinates. Hence the range of importance for $q'$ is as follows:

$$0 < q' \leq \frac{1}{r'}$$

Since we are concerned with all r' for which $r' >> \lambda'_{eff}$, we can safely substitute $\lambda'_{eff}$ for r'. This will only increase the range of integration for $a'_{\varphi}$ beyond the cutoff point where the functions inside the integral reduce to relatively small numbers anyways. The new range of integration is

$$0 < q' \leq \frac{1}{\lambda'_{eff}} << 1$$

In this range,

$$f_1(q') \cong f_1(0) = 1$$
$$f_2(q') \cong f_2(0) = 1$$
$$f_4(q') \cong f_4(0) = 1$$

Now

$$a'_{\phi}(\rho',z') \cong \frac{1}{\kappa} \int_0^{\infty} dq' \; J_1(q',\rho')e^{-q'z'}$$

$$= \frac{1}{\kappa\rho'}\left(1 - \frac{z'}{\sqrt{\rho'^2+z'^2}}\right)$$

$$\vec{b}'(\rho',z') = \frac{-\partial a'_{\phi}(\rho',z')}{\partial z'} \hat{\rho} + \frac{1}{\rho'}\frac{\partial}{\partial \rho'}[\rho' a'_{\phi}(\rho',z')] \hat{z}$$

$$\cong \frac{\rho'}{\kappa(\rho'^2+z'^2)^{3/2}}\hat{\rho} + \frac{z'}{\kappa(\rho'^2+z'^2)^{3/2}}\hat{z}$$

$$= \frac{1}{\kappa r'^2}\hat{r}$$

$$\vec{b}(\rho,z) = \frac{\phi_o}{2\pi r^2}\hat{r}$$

which resembles a monopole field with flux $\phi_0$ evenly distributed over a hemisphere of area $2\pi r^2$ centered on the vortex core and extending above the surface of the film.

In the case of the Nb thin-films I will be examining, $\lambda \sim 860$ Å [5] and $d \sim 2500$ Å. So $\lambda_{eff} \cong 2\lambda^2/d \cong 590$Å. This indicates that any magnetic field sensing device may be safely located to within $6.35 \times 10^{-7}$ $m$ (or $2.5 \times 10^{-5}$ $in.$) of the film while preserving the validity of the monopole field approximation.

## VORTEX TRAPPING ENERGIES

Now that we've ascertained the far-field appearance of a flux vortex for detection purposes, it is important to calculate the potential energy well of a perforation in a superconducting thin film which tends to attract a vortex to its center. First of all, there are three components to the free energy of a vortex relative to the energy of a superconductor in the Meissner state (Clem[6]):

$$F_{tot} = F_c + F_{kg} + F_{em}$$

$F_c$ is the energy due to the loss of superconducting condensation energy in the core.

$$F_c \cong \frac{H_c^2}{8\pi}(\pi\xi^2 d) = \frac{\phi_0^{\,2}}{8\pi^2\lambda_\perp}\frac{1}{4}$$

$$\text{where } H_C = \frac{\hbar c}{\sqrt{2}e^*\lambda\xi} \qquad \text{(DeGennes[7])}$$

$$\phi_0 = \frac{ch}{e^*}$$

$$\lambda_\perp = \frac{2\lambda^2}{d}$$

$F_{kg}$ accounts for the energy it takes to bend the normalized G-L order parameter from 1 to 0 as one moves towards the center of the core. It's the kinetic energy of the gradient of the superconducting wave function.

$$F_{kg} = \int_{V_{film}} dV \frac{\hbar^2}{2m^*} |\nabla\Psi|^2$$

$$= \frac{\hbar^2 \Psi_o}{2m^*} \int_{V_{film}} dV |\nabla f|^2$$

$$= \frac{\phi_0^2}{8\pi^2\lambda_\perp^2} \int_0^\infty r\,dr \left(\frac{\partial f}{\partial r}\right)^2 \cong \frac{\phi_0^2}{8\pi^2\lambda_\perp} \cdot \frac{1}{4}$$

$$\text{where } \Psi = \Psi_o f e^{-i\phi} \quad (\gamma = -\phi \text{ for a vortex})$$

Note that $F_{kg}$ and $F_c$ balance each other. If the superconducting wave function $\Psi$ varied less rapidly, hence lowering $F_{kg}$, $F_c$ would increase because the superconducting electron pair density $n_s^* = |\Psi|^2$ would likewise be reduced in the vicinity of the vortex. If instead $\Psi$ varied more rapidly decreasing $F_c$, $F_{kg}$ would go up.

Lastly, $F_{em}$ is the electromagnetic energy associated with the circulating current density $j'(\rho')$ and the induced magnetic field $b'(\rho',z')$.

$$F_{em} = \frac{-\phi_0}{4\pi c}\int_{V_{film}} dV\, \vec{j}\cdot\vec{\nabla}\gamma$$

Pearl[8] approximated the current density for a thin-film arriving at the expression:

$$\vec{j} \cong \frac{c\phi_0}{4\pi^2\lambda_\perp r}\hat{\phi} \quad \text{in the region} \quad \xi \le r \le \lambda_\perp \qquad \left(\lambda_\perp = \frac{2\lambda^2}{d}\right)$$

Substituting into the previous equation:

$$F_{em} \cong \frac{-\phi_o}{4\pi c}\frac{c\phi_o d}{8\pi^2\lambda^2}2\pi\int_\xi^{\lambda_{eff}} \frac{1}{r}\,dr\left[\frac{1}{r}\hat{\phi}\cdot-\frac{1}{r}\hat{\phi}\right]$$

$$= \frac{\phi_o^2}{8\pi^2\lambda_\perp}\left(\ln\frac{\lambda_\perp}{\xi}\right)$$

The total energy is

$$F_{tot} = \frac{\phi_o^2}{8\pi^2\lambda_\perp}\left(\frac{1}{2} + \ln\frac{\lambda_\perp}{\xi}\right)$$

If one cools a thin film in the presence of a static field, the flux vortices generated assume their final position within a few milli-degrees below $T_c$[9]. Since $\lambda >> \xi$ near $T_c$, the $F_{em}$ term dominates $F_{tot}$ and provides the main contribution to the total energy.

In the case of a perforation or "hole" in a thin film, Bermon and Clem [10] have shown this provides a potential energy well for a vortex. If the hole containing a vortex is circular with radius $a$, current cannot flow for $r < a$, and so the lower level of integration for $F_{em}$ is $a$ instead of $\xi$

$$\Delta F_{hole-film} = \frac{\phi_o^2}{8\pi^2\lambda_\perp}\left(\ln\frac{\lambda_\perp}{a} - \ln\frac{\lambda_\perp}{\xi}\right)$$

$$= \frac{-\phi_o^2}{8\pi^2\lambda_\perp}\ln\frac{a}{\xi}$$

$\Delta F_{hole\text{-}film}$ is a negative restoring energy attracting the vortex to the hole.

It is difficult to analyze accurately more complex hole structures (such as rectangular slits or other angular constructs) using the above model. The current distribution of a trapped vortex in such a hole is difficult to calculate. However, the flux scanner as envisioned by S. Bermon[11] will provide a means to analyze such structures because one will be able to experimentally ascertain trapping probabilities for various hole configurations.

## NOTES

1. J. Pearl, Journal of Applied Physics **37**, (1966) pp. 4139

2. J. R. Clem, Journal of Low Temp. Physics **18**, (1975) pp. 427

3. After J. R. Clem, Journal of Low Temp. Physics **18**, (1975) pp. 429

4. J. R. Clem, Proceedings of the Conference on Inhomogeneous Superconductors - 1979, Edited by D. U. Gubser, T. L. Francavilla, J. R. Leibowitz, and S. A. Wolf, (American Insitute Of Physics, New York, 1980), pp. 245-50.

5. W. H. Henkels and C. J. Kircher, IEEE Trans. on Mag. **13**, (1977) 63

6. J. R. Clem, Proceedings..., pp. 245-50.

7. P. G. De Gennes, Superconductivity of Metals and Alloys, W. A. Benjamin, Inc., (1966) pp. 60

8. J. Pearl, Applied Physics Letters **5**, (1964) pp. 65

9. S. Bermon, private communication.

10. S. Bermon and J. R. Clem, private communication through S. Bermon.

11. S. Bermon, private communication.

# CHAPTER III: FLUX SCANNER DESCRIPTION

## INTRODUCTION

The basic operation of the flux scanner breaks down into five component pieces which I shall briefly outline before the detailed descriptions begin.

First of all, there is a mechanical assembly (MA) which can move the planar surface of a quarter-inch square superconducting thin film past a stationary probe, while maintaining a constant separation distance of .002 inches between the probe and the film. Of course, the movable parts of this assembly must be operable at liquid He temperature, so they must be free of all dirt, grease, and water vapor. This necessitates the enclosure of the MA in a vacuum-tight, partially evacuated chamber. The MA also has a heater assembly around the chip position, so that after lowering the assembly into the LHe, the chip can be heated above $T_c$ in the presence of a finely-controlled incident field. Upon re-cooling through $T_c$, the magnitude of this ambient field normal to the film's surface will determine the population of flux vortices in the superconducting thin film.

Secondly, there is a multi-turn sense-coil (referred to as "the probe") which is placed next to a thin film within the MA. Its oriented so that magnetic flux emanating from trapped vortices will pass through the coil, generating a current in the coil wire, as the MA moves the chip past the probe. The two leads from the sense-coil are attached to a S.H.E.[1] SQUID ("SQUID" stands for Superconducting QUantum Interference Device). This SQUID is an ultra-low-noise current sensing device which operates at liquid He temperature and outputs a voltage level proportional to input current. The voltage output from the SQUID is thus proportional to the flux passing through the sense-coil, and can be used to drive one axis of an x-y plotter which plots magnetic field versus position.

Thirdly, there is a digital/analog circuit which controls the two motors in the mechanical assembly which in turn control the y-z positioning of a superconducting thin film next to the sense-coil probe. (The probe's axis is in the x-direction.) The electronics have a manual mode where a point on the chip can be swept directly to a desired location next to the probe, and an automatic mode which will sweep the chip in a raster pattern past the probe.

Fourthly, a shielding system inside the dewar provides a low-field environment for the lower part of the mechanical assembly, where the sense-coil and thin film sit. The purpose of this system is to accurately control the number of flux vortices trapped in a thin film, when it is cooled through the superconducting transition temperature. This system also tries to ensure that the distribution of flux across a film is uniform, and that field fluctuations in the outside environment will not destroy this uniform, low-field environment.

Lastly, the final piece of the flux scanner is the set of two chips designed and fabricated to test the operation of the whole device. These chips consist of a layer of Niobium deposited on a silicon surface with a regular array of holes etched through the superconducting metal. These chips were successfully used to trap flux vortices at predetermined sites, enabling the flux scanner to observe and record their presence.

Each of these component parts of the flux scanner will be discussed in further detail in the following sections.

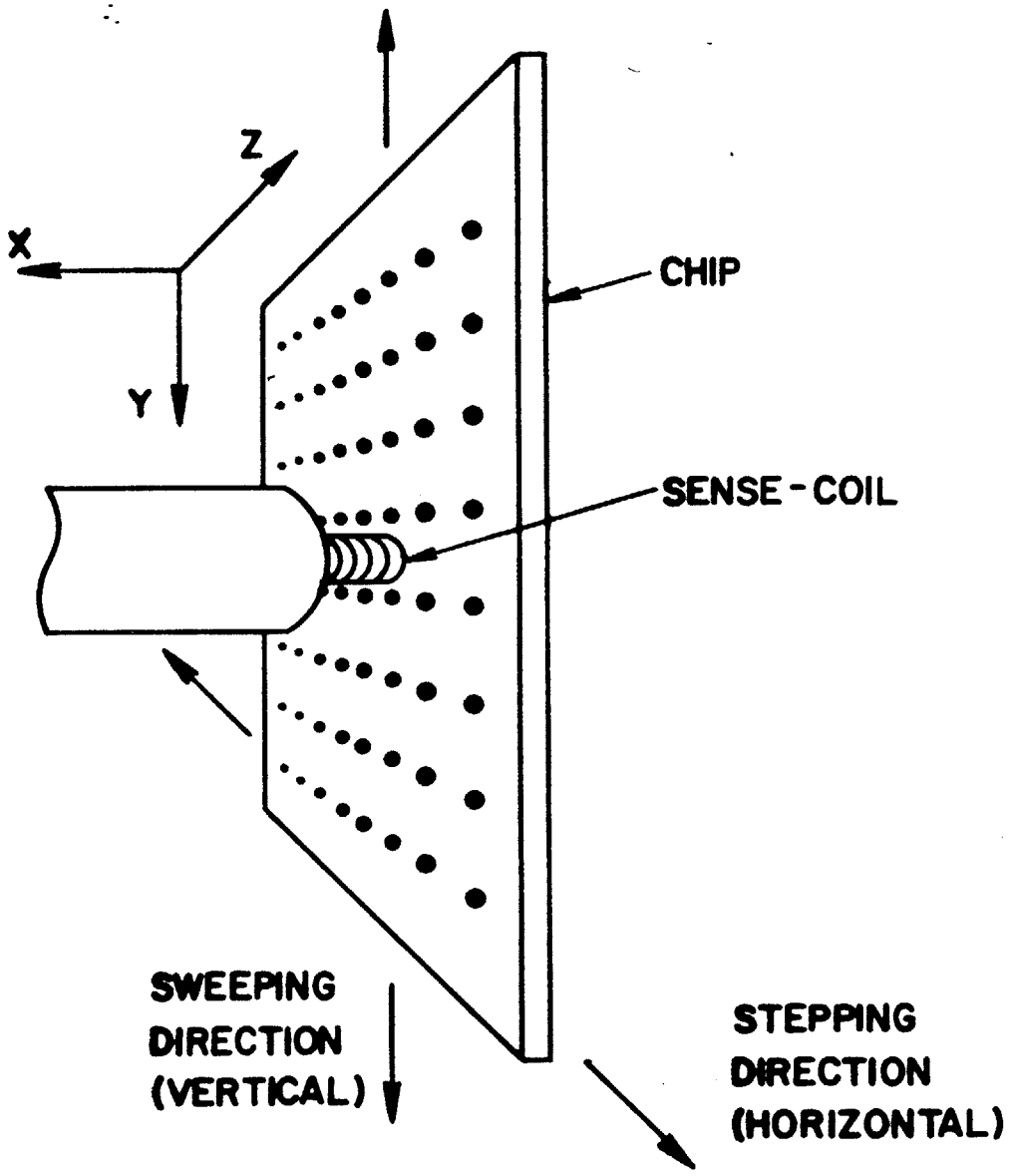
Z
X
Y
CHIP
SENSE - COIL
SWEEPING
DIRECTION
(VERTICAL)
STEPPING
DIRECTION
(HORIZONTAL)

FIGURE 4

## MECHANICAL ASSEMBLY

The purpose of the mechanical assembly (referred to as the MA) was to achieve spatial resolution in the three-dimensional positioning of a field sensing probe next to a test-chip (See Figure 4). We defined the three components of the 3D positioning as follows: the x-position is the separation distance between the chip and probe, the y-position is the vertical coordinate of the moving chip with respect to the stationary probe, and the z-position is the horizontal coordinate of the moving chip with respect to the probe. The maximum resolution achievable in each direction was extremely important because flux vortices are incredibly small compared to the size of the mechanical components we dealt with. The detection of these vortices hinge upon precise, mechanical motion.

### Materials

Our first concern was to construct the mechanical assembly out of materials that would not generate a large remanent field in the test chip position. A remanent field could possibly generate unwanted vortices when cooling a chip through $T_c$. Its presence could also confuse attempts to observe vortices trapped in a chip, especially if the remanent field emanated from a moving part. For these reasons, we attempted to use non-magnetic materials such as aluminum, teflon, brass, and stainless steel (only when necessary). Within 8" of the test chip position, we only used aluminum. The table below gives the remanent field associated with the various materials we used in the construction of the flux scanner[2]. Our goal was to maintain the gradient of this remanent field below 1$\mu$G across the plane of the chip. The absolute field could always be nulled with coils. Later measurements of the flux scanner apparatus without the probe-arm and probe mount table attached, confirmed that we had come close enough to achieving this goal to proceed with experimentation.

| | $4\pi M$ (gauss) | Vol. ($cm^3$) |
|---|---|---|
| Aluminum: 6061-T6 | $4.7\times10^{-7}$ | 0.201 |
| Brass: rod stock | $9.7\times10^{-4}$ | 0.113 |
| Steel: 304 stainless tube | $4.4\times10^{-3}$ | 0.0227 |
| soft steel rod | $1.9\times10^{-1}$ | 0.00036 |
| Teflon: rod stock | $3.6\times10^{-6}$ | 0.201 |
| Phenolic: cloth filled | $1.6\times10^{-6}$ | 0.113 |
| Copper: #33 wire formvar ins. | $3.3\times10^{-5}$ | 0.00525 |
| Evanohm: #28 wire silk ins. | $5.2\times10^{-5}$ | 0.0083 |
| Manganin: #30 wire forex ins. | $1.7\times10^{-5}$ | 0.0125 |

**Precision Movement of Probe-Arm**

The field emanating from a single trapped vortex in a smooth superconducting film largely dictates the exact resolution requirements of the probe-arm movement. In order to fully understand these requirements, it is useful to look closely at the field produced by a single vortex, and the flux detecting apparatus available. Once we understand these factors, it is readily apparent how precise our mechanical movement has to be.

As developed in Chapter 1, the far-field appearance of a flux vortex resembles that of a magnetic monopole. The detection apparatus I used consisted of a multi-turned annular sense-coil attached to a SQUID. We can assume for the moment that the minimum flux from a vortex we must couple into the individual turns of the sense-coil is about $0.1\phi_0$. This is the minimum flux required to produce an acceptable signal-to-noise ratio at the SQUID output terminals. Looking at Figure 5 on the following page, the flux coupled into a single loop with radius $c$ spaced a distance $d$ away from the film, is given by the simple expression:

$$\psi_{loop} = \phi_0\left(1 - \frac{d}{\sqrt{c^2 + d^2}}\right)$$

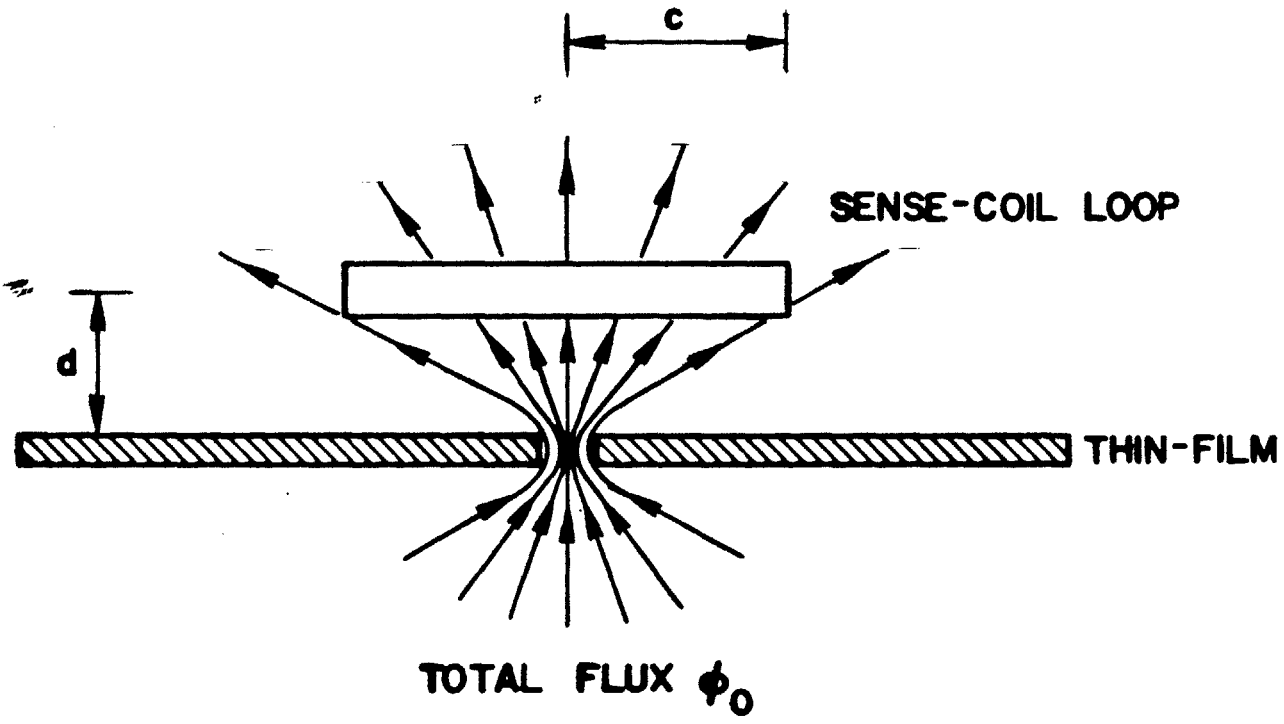


FIGURE 5

$$\phi_0 = 2.07 \times 10^{-7}\ G - cm^2 \quad (1 \text{ flux quantum})$$

Since we want to make the resolution of the sense-coil as fine as possible, the obvious choice is to make $c$ as small as possible. The loop radius is constrained, though, by the minimum size of the coil form on which it can be wound. The minimum thickness of commercially available Niobium wire is about .0025 inches (.002 inches in diameter with a .00025 inch coating of insulation), so in order to ensure that the Formvar insulation won't crack, it must be wound on a diameter no less than .009 inches. This constrains the variable $c$ in the above equation to a value greater than .0045 inches. If we choose d = .00325 inches, this means the actual spacing between the loop and film is about .002 inches. The extra .00125 inches accounts for the radius of the .0025 inch thick NB wire. Plugging these values for $c$ and $d$ into the above equation, we find $\Psi_{loop} = 0.41\phi_0$ This is well within our requirement of $0.1\phi_0$ per loop. Now we'll be able to wind additional loops above this one, further away from the chip surface, but still within range to capture a tenth of a flux quantum. Winding additional loops will improve our signal to the SQUID. Thus, a vertical spacing of .002 inches seems a good figure to aim for.

So far, in our flux calculations, the loop radius $c$ appears to be the constraining factor determining the maximum allowable spacing between the sense-coil and the film surface. We already decided that the minimum loop radius was .0045 inches, and we used that figure to calculate the maximum vertical spacing of .002 inches. Now we should discuss why minimizing the loop radius $c$ is essential to ensure a fine-grained planar resolution. With the flux scanner we will be examining vortices trapped in dense thin-film structures. The smaller the sense-loop radius, $c$, the sharper the peak produced by a vortex passing over the sense-coil. Assume that, moving the vortex several diameters away from a position directly centered over the loop, will result in a vanishingly small signal from the vortex as compared to the signal in the centered position. (Of course, we're still assuming the monopole condition, $c >> \lambda_\perp$, were $c$ is the loop radius, and $\lambda_\perp$ is the "monopole radius".) Then, the smaller the loop diameter, the

sharper the falloff as it passes over the location of a vortex, and the better the resolution when scanning a thin-film.

This finer planar resolution in the design of the loop must however be matched by the resolution of the MA's scanning mechanics in order to be useful. To take full advantage of the minimum $c$ = .0045 inches, the movement of the MA must be spatially accurate at least to within ±.002 inches. This initial assumption provides for a vortex in the chip to be misaligned from the probe by a quarter of a loop diameter while still detecting an acceptable vortex signal level. This seems reasonable in light of our calculations above. As for a ballpark resolution for the .002 inch vertical spacing, ±.0005 inches appears to be an appropriate number. The flux passing through a loop spaced .002 ±.0005 inches only varies by ±15%. Although the resolution calculations we made here are somewhat arbitrary, they gave us some rough estimates when we first started building the flux scanner. This provided a basic understanding of how precise our mechanical design would have to be.

For the y-z planar motion we employed screw-motion slides which translated the rotational movement of the drive shafts into the linear movement of the slides. (See Figure 6 on the following page.) Since the electric motors providing the power to the sliders had to operate at room temperature, we used long drive shafts to connect the motors to the slides through the dewar neck. To achieve planar motion, one slide was mounted perpendicularly on top of the other. One slide controls the vertical motion of the probe-arm, while the other slide controls the horizontal movement of the probe-arm. Thus, one drive shaft makes a straight connection to the vertical slide. The other drive shaft has a bevel gear to turn the direction of the shaft 90° to make the connection to the horizontal slide. Also, this shaft controlling the horizontal motion has a spline in it so that the shaft can extend and contract as the vertical slide moves up and down. In the scanning mode, one shaft turns continuously, reversing direction each time the slider reached the end of its travel inside the slide. The other shaft only turns incrementally, rotating a small fixed amount each time the first shaft reverses direction. In

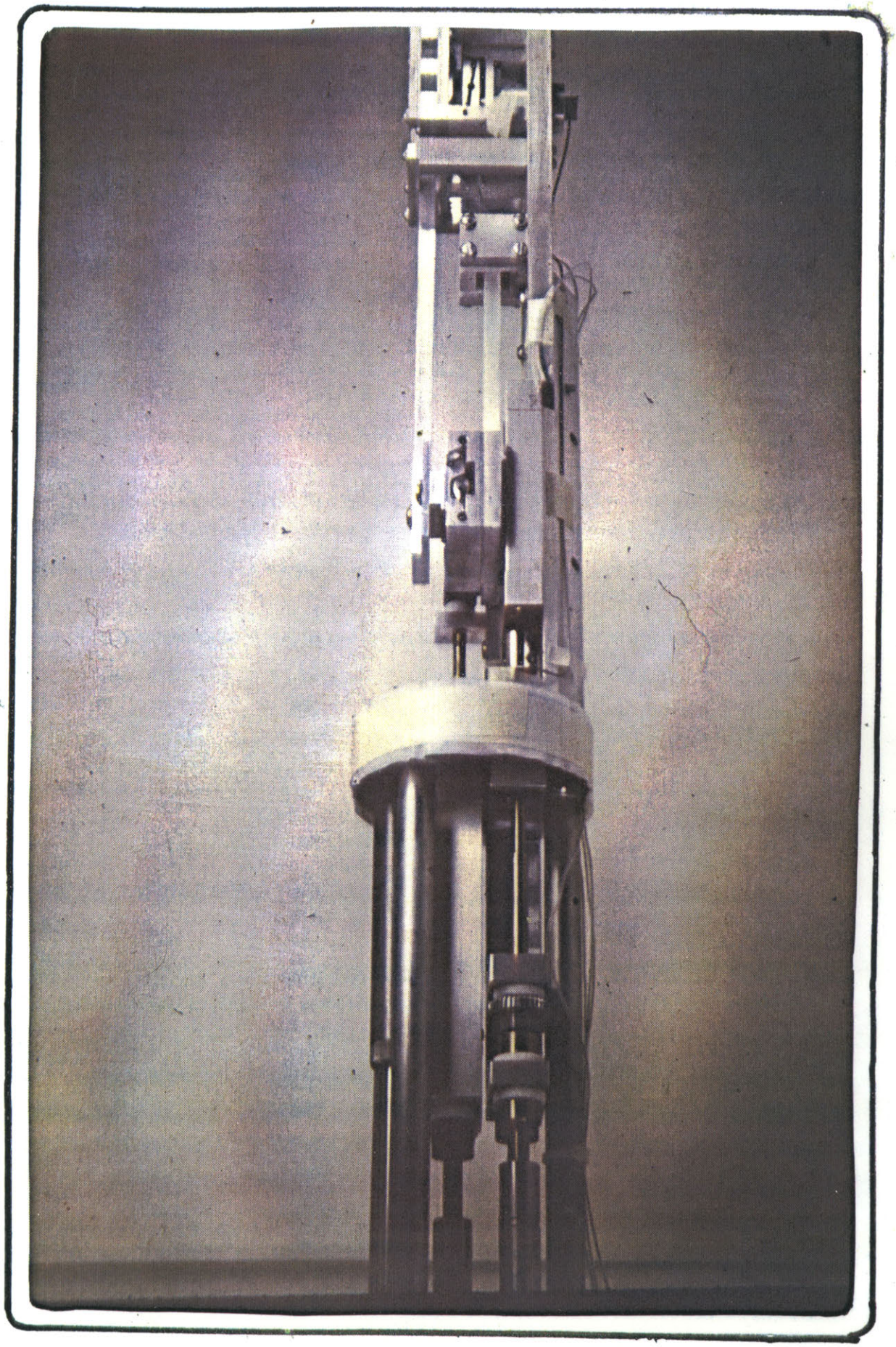

FIGURE 6

this manner the probe arm moves in a raster pattern-- The first slider moves up and down continuously while the other slider moves a small incremental amount each time the first slider reverses direction. Because the vertical slider apparatus is sturdier, (i.e. no bevel gear and spline), it was designated as the continuously moving slide.

Because of the long, cylindrical shape of the dewar neck, the flux scanner was built in a cylindrical fashion. It's overall length from the motor mount plate to the bottom of the mechanical assembly is 47 1/4 inches with a cross-sectional diameter of 3 1/4 inches. The axles had to be made sufficiently long in order to span the length of the dewar neck and position the slide assembly deep in the Helium reservoir. In addition, a cylindrical superstructure with three stainless steel support rods connects the motor mount plate outside of the dewar to the slide assembly inside the reservoir providing a sturdy housing for the long drive shafts. Both the support rods and drive-shafts are made out of thin-walled 3/8" stainless steel tubes for maximum strength and minimal heat conduction between the liquid helium and the outside environment.

In addition to the two drive shafts, there are also two other shafts extending the length of the mechanical assembly. Each of these is connected, through a 1:1 gearing, from the bottom of the drive shafts to the axles of two rotary potentiometers just below the motor mount plate. These are made from 1/4" stainless-steel thin-walled tubes. They are connected to the drive shafts near the point at which the drive shafts connect to the slides. This way, if any rotational twist builds up in the drive shafts due to excessive torques, the feedback pots will not record any angular error at the top of the shafts, instead recording the true position of the slides. As it turns out, backlash in the gears connecting the drive shafts to the feedback shafts, exceeded any rotational twist, so these feedback pots probably could've been connected directly to the drive shafts near the top of the assembly. (Our solution to the backlash problem will be discussed further in the "Electronics" section.)

The slides we use consist of an aluminum slider and an aluminum body. Pads, made from a teflon compound and attached to each slider, ensure smooth, precise motion. The worm screws, which move the sliders within the body, have a pitch of 20 threads per inch. For a 2 mil (= .002 inches) movement the shafts turn $\cong 14°$. This is manageable because the motors can be easily pulsed so that they turn the shaft to within $\pm 3°$

The motors are brushless DC servo-motors with gear heads of 1:540 and 1:360 for the horizontal and vertical directions respectively. Since, at operating speed, it takes $\cong 1$ sec to turn a shaft 14°, timing chips were easily employed for precise control of the shaft movement. Also, the gear heads provide much more resistance to the motors than the flux scanner mechanical assembly, due to the high gearing ratio, so the uniform, continuous load of the gearheads smooth over any "stick points" associated with the rotating shafts in the mechanical assembly. Acceleration and decceleration of the motors is determined by the uniform load of the gear heads as well, so accurate, reproducible shaft movements are possible without using elaborate stepping motors.

**Probe To Chip Spacing**

Besides precise y-z planar motion, the mechanical assembly also answers the need for accurate, adjustable spacing between the probe and a test chip. In order for the probe to "see" the entire surface of the 1/4" square chip, the chip has to able to move 0.375 inches in two directions while maintaining a $2 \pm 0.25$ mil spacing between the coil and the chip surface. As discussed earlier, this coil-to-chip spacing affects the amount of flux from a vortex threading the sense-coil. So for an accurate reading when scanning a 375 mil square range, in which all flux vortices present will generate the same characteristic trace, constant spacing is crucial.

To achieve constant spacing, a probe arm shaped like a cross is supported by four brackets, one for each arm of the cross. (See Figure 7 on the following page.) These

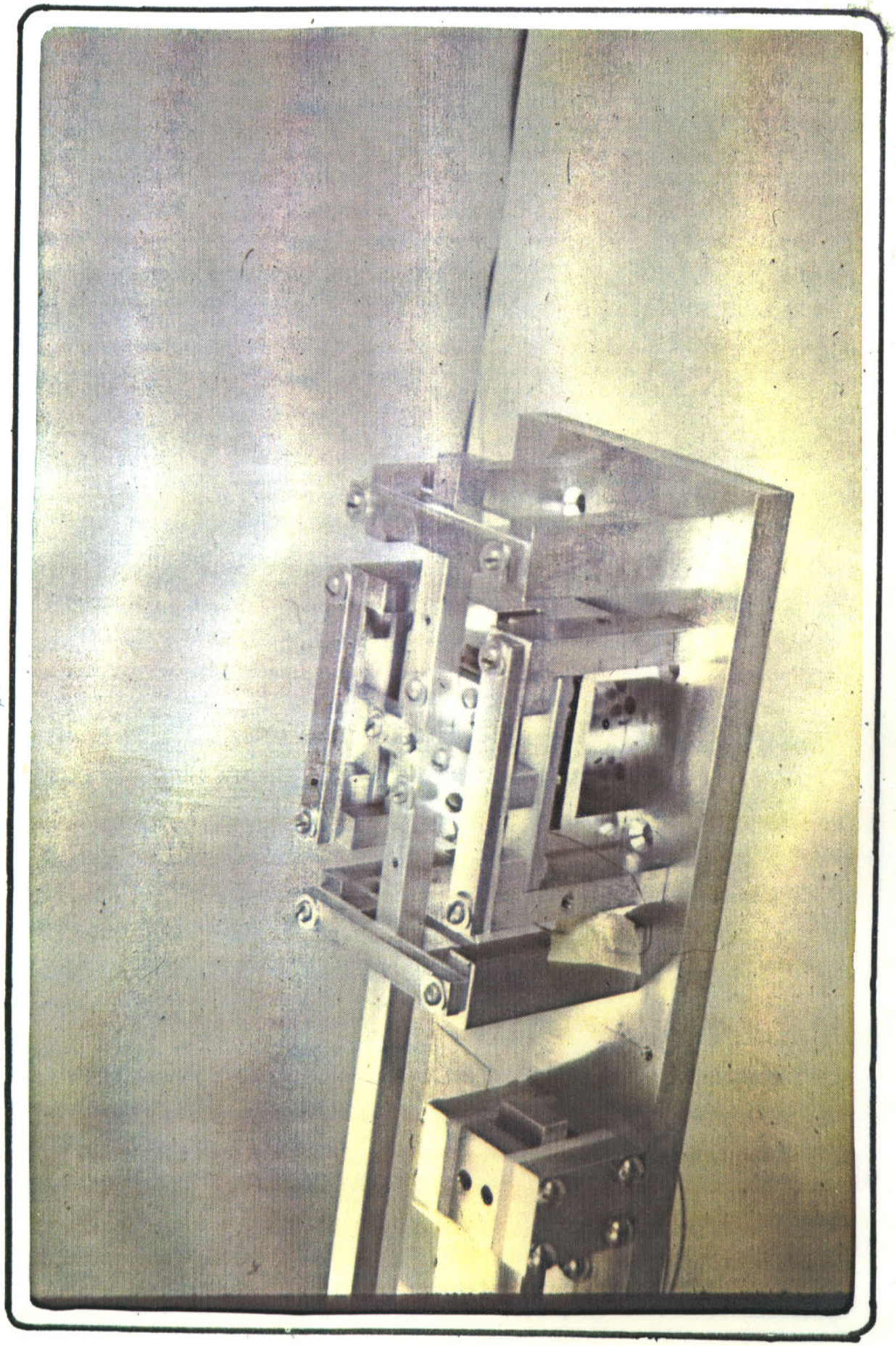

FIGURE 7

brackets enable the cross to move within a .375 inch square plane, while supporting each arm of the cross from both above and below, so that the .002 inch resolution is ensured. Thus, the cross was constrained to move within a plane almost exactly perpendicular to the axis of the stationary sense coil. By adjusting the four brackets, one can selectively raise or lower each arm of the cross with respect to the sense-coil, to make sure the chip stayed within this plane throughout the probe-arm's entire range of operation. One could also tighten each respective bracket around each arm of the cross, to hold it steady and firm. For a smooth sliding surface within each bracket, I used thin teflon strips backed by aluminum. It turns out the thinner the teflon strips the better. Teflon shrinks about 20 parts per thousand between room temperature and 4.2 $^{\circ}K$ (Liquid Helium temperature), so for the 1/16" thick strips we used, they each shrunk only about 1 mil in thickness. By over-clamping each bracket around each arm of the cross before cooling, we could compensate for this 1 mil shrinkage. When the system cooled down, the brackets would loosen slightly to just the right clamping pressure, at which the cross moved with maximum steadiness and minimal friction. This system turned out to work quite well at liquid He temperatures.

As for making fine adjustments to the spacing between the chip and sense-coil, I built an adjustable table with a 40 threads per inch lead screw controlling the height of the table. (See Figure 8) This made it relatively simple to raise and lower the sense-coil with respect to the chip attached to the probe arm. Here I also had to account for thermal contraction. When conducting experiments, I had to space the sense-coil and chip by .005 inches before cooling, using a floor microscope. After cooling, judging from the SQUID response, the sense-coil to chip separation contracted to about .002 inches. This final separation distance proved to be an optimal spacing, for it provided an adequate signal-to-noise ratio when passing over a vortex, while keeping the sense coil from accidentally touching the chip. If the sense coil did touch the chip, they would short together, causing the SQUID to lose its equilibrium feedback position, and oftentimes causing damage to the sense-coil.

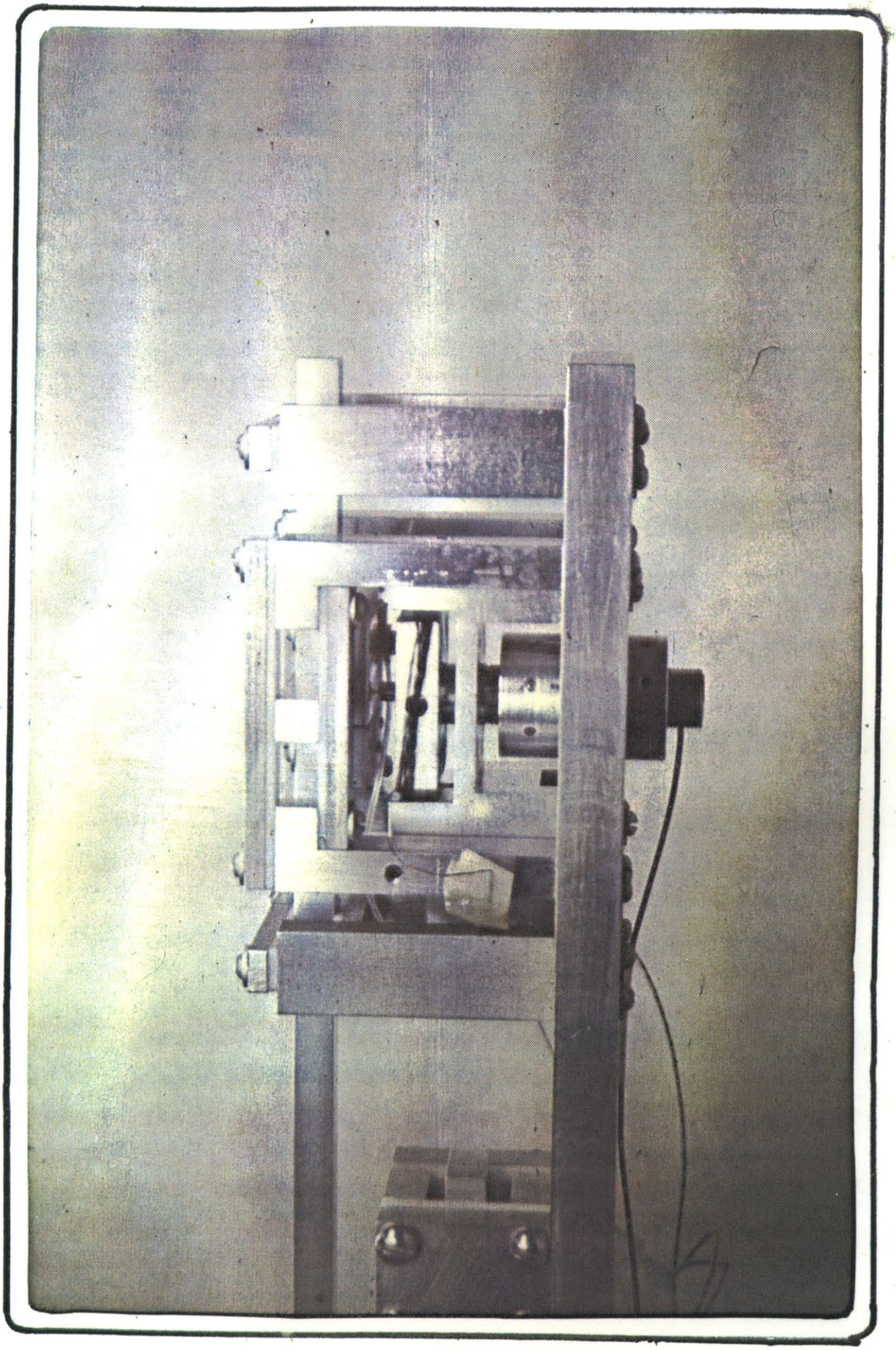

FIGURE 8

It was also necessary to align the chips perfectly parallel to the probe arm when mounting them. Otherwise, the steps taken to make the probe arm movement "isoplanar", would be futile. Here there were two items of concern. First, the chip had to be correctly mounted to an aluminum backing plate. Then, this backing plate had to be carefully screwed onto the probe-arm. For mounting the chip to a backing plate, I tried several different adhesives which could endure thermal cycling between 4.2 $^{\circ}K$ and 300 $^{\circ}K$. I achieved satisfactory results only with General Electric 7031 Varnish, an insulating material often used for coating coil windings. It could be applied in extremely thin coats, and dried to a hard finish when heated. The GE Varnish also endured heavy stresses set up by the dissimilar coefficients of contraction between Al and Si. (Al contracts 4 parts/thousand between 4.2 $^{\circ}K$ and 300 $^{\circ}K$ while Si contracts only 0.2 parts/thousand.) To partially distribute these stresses over a relatively large volume of varnish, I configured the backing plates with a small dimple about .020 mils deep in the center where a drop of GE Varnish could be placed. After drying, this drop provided a large volume of adhesive, bonding the chip firmly to the precision-milled backing plate, whereas a thin layer between the chip and backing plate would not have held at 4.2 $^{\circ}K$. Oftentimes imperfect gluing of the chip to the backing plate resulted in a relatively large .001 to .005 inch error in parallelism between the chip and probe-arm over the width of the chip. This was solved by shimming the backing plate with respect to the probe with thin brass shim material. By watching the chip move back and forth over the sense-coil, and carefully estimating their spacing, one could shim the backing plate until the coil-to-chip spacing was accurate to within $\pm$ 0.00025 inches. (A floor microscope provided great assistance to me when estimating the probe to chip spacing.)

**Fiducial Lines**

The fiducial lines are a means of orienting the chip with respect to the probe when the flux scanner is immersed in a Helium bath. They provide a calibration for the probe while the system is in operation. A drawing of the fiducial lines is given below (Figure 9). They are

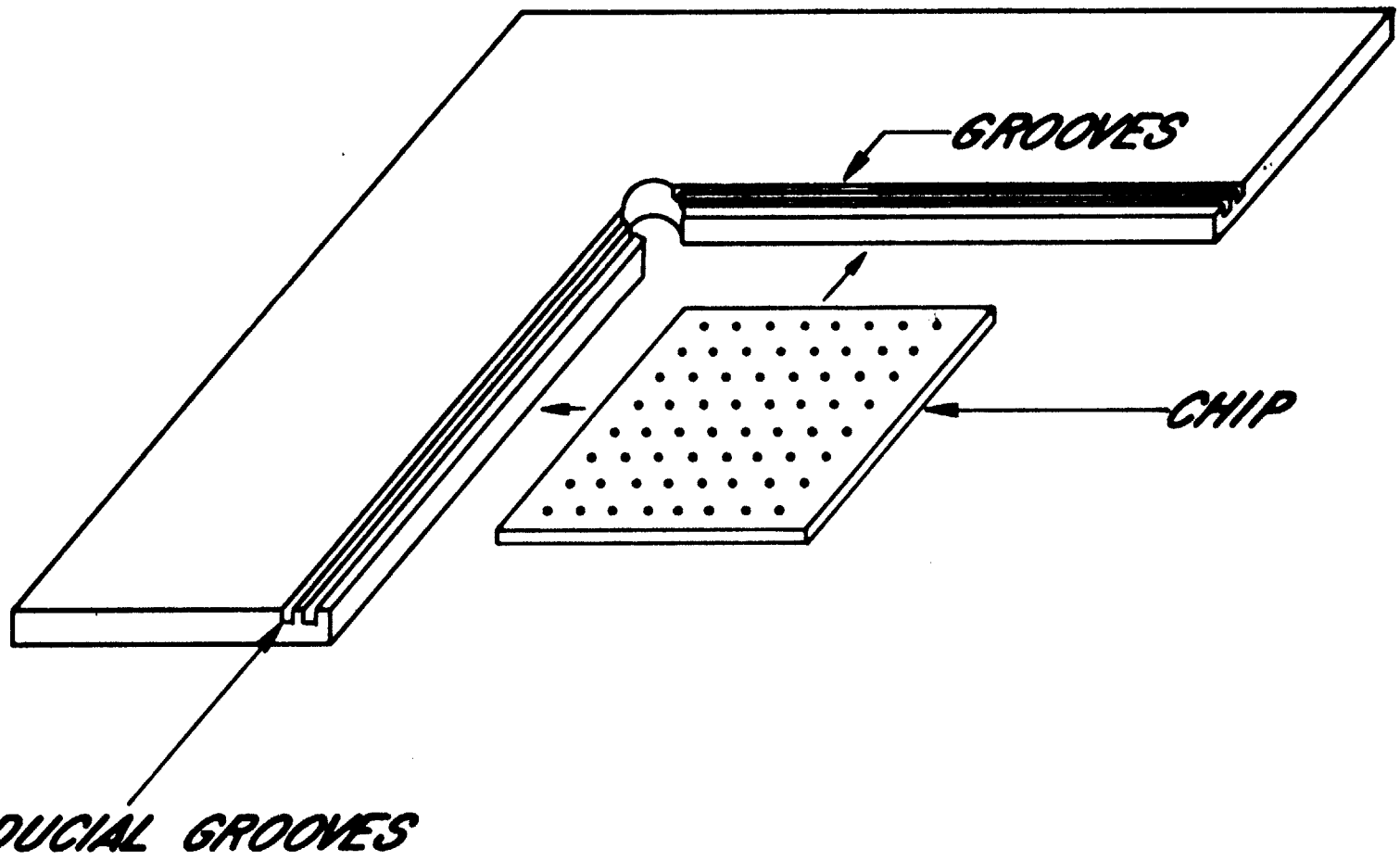


FIGURE 9

actually a single 0.002 inch diameter Nb wire which fits into two parallel grooves cut into an Al L-shaped block. The wire runs down one groove and back up the other, so that when a current passes through the wire, the resulting magnetic field will be sharply peaked at the midpoint of the two wires. In normal operation of the flux scanner, a chip will be positioned against the inside edge of the L-shaped block. The fiducial lines near the edge of the chip will generate a calibration signal as the chip scans over the probe. They will not only tell where the edge of the chip is, but they will also give an idea of the relative spacing between the probe and the plane of the chip.

I cut the fiducial grooves using a diamond saw which normally dices silicon wafers into chips. This saw afforded very good control on the groove spacing and groove depth. Dimensionally, the grooves' midpoint was 18.5 mils from the L-block edge and they were spaced by 7 mils. The groove width and depth were each 3 mils. GE Varnish held the 2 mil superconducting Nb wire into the grooves, and I spot-welded 7.43 ohm/ft. Manganin wire onto the two superconducting leads. Manganin wire has a lower thermal conductivity than copper, so it was appropriate to use for connecting the fiducial lines to a current source outside the dewar.

The primary advantage of using superconducting wire in the grooves was the fact that electrical shorts at room temperature between the L-block and the fiducial lines disappeared upon cooling to 4.2 $^{\circ}K$. When the fiducial lines became superconducting, current would no longer flow through the L-block, even if the insulation on the Nb wire scraped off when inserting the wires into the grooves. This turned out to be a significant advantage, especially since it was difficult enough just to insert wires into the grooves without ensuring electrical isolation.

The field emanating from the fiducial lines was especially valuable as a calibrator for the sense-coil. I derived the following expressions from which I could numerically calculate the flux passing through each loop of the sense-coil. From this, I could arrive at an order of magnitude figure for the SQUID output signal. I could then check this calculated result with

my experimental observations which would tell me if the sensitivity of the sense-coil met my expectations. The following formula calculates the incremental area of a sense-coil loop between $d_1$ and $d_2$, as shown in the accompanying diagram (Figure 10).

$$A_i = r^2(\theta_2 - \theta_1) + rd_1 \sin\theta_2$$

$$\text{where} \quad \theta_j = \cos^{-1}\left(\frac{d_j}{r}\right)$$

This formula gives the vertical component of the $B$ field through each area element of a sense-coil loop calculated above.

$$\vec{B}_{yi} = \frac{\mu_o I x_1}{2\pi(x_1^2 + h^2)} - \frac{\mu_o I x_2}{2\pi(x_2^2 + h^2)}$$

$$\text{where} \quad x_j = \left(\frac{d_1 + d_2}{2}\right) + (-1)^{j-1} a$$

Using

$$\Psi_{sense-coil} = \sum_{\forall loops}\left(\sum_i A_i \vec{B}_{yi}\right)_{loop}$$

one can calculate the amount of flux from the fiducial lines through the sense-coil, at any position of the sense-coil, as long as it's axis is perpendicular to the plane of the fiducial lines. Although I did these calculations by hand, choosing a large incremental distance between $d_1$ and $d_2$ to shorten the computation time, this could easily be done more accurately on a computer by choosing a smaller incremental distance.

While waiting for the test chips to be fabricated, I was able to use the fiducial lines as a guide for sense-coil design. Although the field from the fiducial lines decays as $1/R$, and a vortex field decays as $1/R^2$, the fiducial lines were still experimentally useful. With them, I checked several assumptions about the behavior of my sense-coils, and was also able to evaluate the practicality of a superconducting transformer between the sense-coils and the

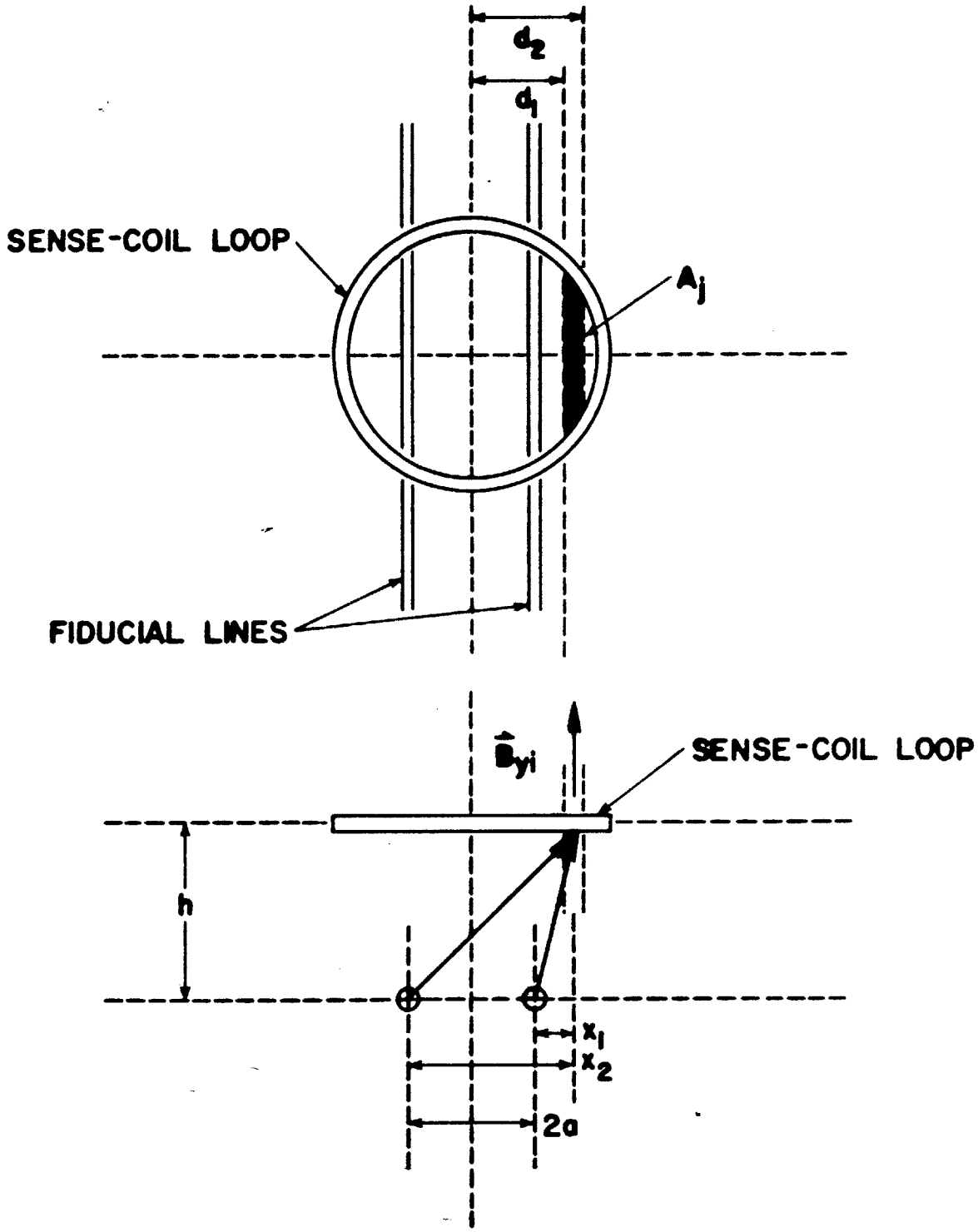
$d_2$
$d_1$
SENSE-COIL LOOP
$A_j$
FIDUCIAL LINES
$\hat{B}_{yi}$
SENSE-COIL LOOP
h
$x_1$
$x_2$
2a

FIGURE 10

SQUID input loop. The results of these preliminary experiments will be discussed in Chapter IV.

**Evacuation**

To operate the flux scanner successfully, a clean environment is necessary. All moving parts have to be cleaned beforehand in an ultrasonic freon degreaser. This cleaning removes all grit and grease which can freeze the apparatus and render it inoperable at 4.2 $^{\circ}K$. (This cleaning also removes any magnetic dust which could generate unwanted vortices in the thin-film.) The entire apparatus below the motor mounting plate is also encased in a 95 mm. O.D. pyrex tube. This tube is vacuum tight and must be pumped down to below 5 microns of Hg using a diffusion pump for several hours. This step removes all water vapor which might otherwise cause the drive shafts to freeze up. The tube is then backfilled with a He exchange gas to about 500 mm. of Hg. This exchange gas ensures good thermal contact between the helium bath and the superconducting materials used in the Flux Scanner.

As for passing the drive shafts and electrical lines from the vacuum to the outside world, we used several methods. For the vertical control axle feedthrough between the vacuum and outside world, we employed a Temescal sealed bellows 1/4" shaft rotary feedthrough. This was an expensive but 100% guaranteed method of isolating the evacuated chamber from the outside world. Earlier, I'd tried to use a rotary feedthrough which employed O-ring seals, but this leaked profusely with the continuously turning axle. For the horixontal control axle, which turned only slightly each time the vertical axle reversed direction, I was able to successfully use an O-ring seal heavily greased with silicon lubricant. For the electrical feedthroughs, I used a 24 pin hermetically sealed electrical connector. There were 16 signal lines in all passing through to various devices inside the glass tube. And finally, there were three needle valves attached to the evacuated chamber. One was used for a pumping port, one was used to

attach a pressure relief valve and a thermocouple gauge, and the last was used to bleed in the exchange gas.

**Heater Assembly**

In the mechanical assembly, a heater is necessary in the vicinity of the chip. The chip can then be cooled in any ambient field desired. This allows for multiple flux trapping trials at a single field value or at many different field values. Physically, the heater consists of a six foot length of 50.15 ohm/ft. Evanohm wire, folded in half, and twisted together. This ensures that when a current passes through the wire, the external field generated will be very small. The twisted wire is wound around the probe-support table directly under the chip and fiducial lines. Like the fiducial lines, a 7.43 ohm/ft. twisted pair connects the heater to the outside world.

Since the entire assembly is in a Helium exchange gas, the chip heats through gaseous conduction. The probe-support table is not directly attached to the chip, and so the twisted pair heats the table, which in turn heats the chip through the exchange gas. One way I found to test whether the chip was being heated above $T_c$, was to detach the probe from direct thermal contact with the probe-support table, and see if the sense-coil went normal under an applied current to the heater. If the SQUID response decayed totally from an equilibrium position, one could be assured that the exchange gas in the vicinity of the sense-coil had passed $T_c$ for Nb. Since the thin-film on the chip was Nb as well, it was reasonable to assume the chip had heated also. Generally, I found that $>4W$ of power had to be supplied in order to heat the chip. At exactly $4W$, about 75 sec was needed to both heat and recool the chip.

Also, it is important to note that the field produced by the heater perpendicular to the plane of the chip was checked using the flip-coil magnetometer. I found that the heater did not visibly produce fields in excess of 0.5 $\mu G$ (i.e. not enough to produce one flux quantum across the area of the chip).

**Flip-Coil**

The intention of the flip-coil is to be able to measure the ambient magnetic flux in the exact chip position within the flux scanner apparatus. In actual operation, the flip-coil is attached to the SQUID in lieu of the sense-coil. The actual coil is rectangular in shape and 1/4" on each side-- the exact size of a typical chip. Three gears translate the motion of the horizontal control axle to another auxiliary axle in the plane of the chip. (The horizontal control axle has to be detached from the horizontal slide when the flip coil assembly is attached to the flux scanner.) This auxiliary axle rotates the actual flip-coil. The self-inductance of the flip coil is 2 $\mu H$ which matches the inductance of the SQUID input loop. This precise matching of inductances is optimal for coupling a maximum amount of flux from the flip-coil to the SQUID input loop. Figure 11 on the next page shows a picture of the flip-coil in its operating position.

The flip coil works as follows. Since the SQUID records changes in magnetic flux, a change in the flux through the flip-coil is registered at the SQUID output terminals. Now, if one takes a SQUID reading when the flip-coil's axis is exactly perpendicular to the plane of the chip, and then one takes another reading with the flip coil spun 180°, the difference between the two readings is exactly twice the absolute magnetic flux through the flip-coil. Thus, with the flip-coil in the exact chip position, one can precisely determine the magnetic flux that would pass through the chip itself! This helped considerably when I was trying to null remnant fields due to the shielding and flux scanner apparatus. Also, I used NbTi wire, with a transition temperature several degrees above that of a Nb thin-film, to wrap the flip-coil. This allowed me to check the field produced by the heater in normal operation without causing the flip coil to go normal.

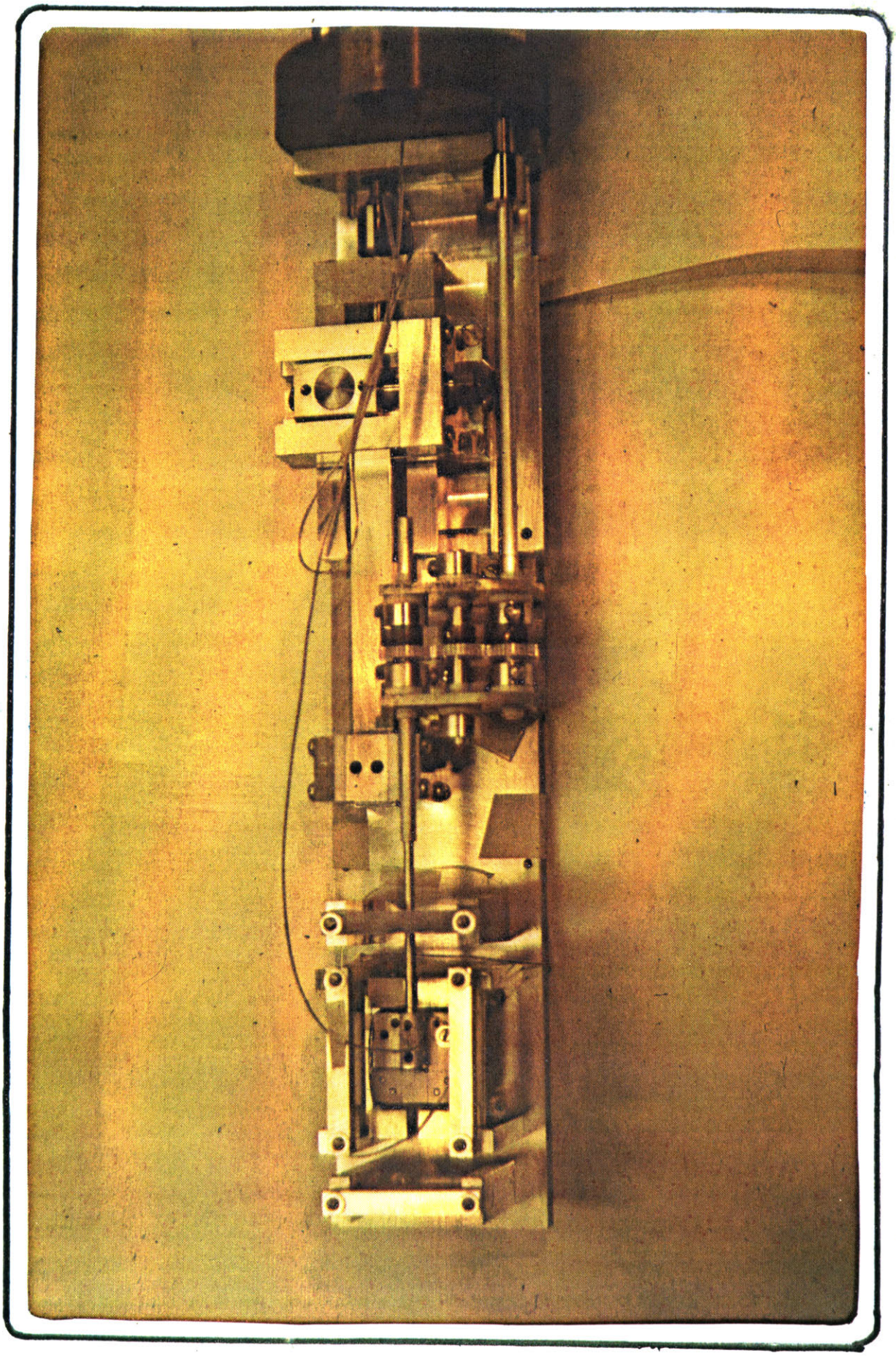

FIGURE 11

## ELECTRONICS

The general idea behind this part of the flux scanner was to automate the chip-scanning process. In order to take data quickly and reliably, we designed and built a digital/analog circuit to operate the mechanical assembly, read the SQUID output, and plot the results on an X-Y Plotter. On the following page is a picture of the front panel of the flux scanner electronics (Figure 12).

### Analog Motor Control

This first part of the circuit, referred to as the "Interface", basically communicates with the two feedback potentiometers and the two DC motors in the mechanical assembly. The feedback pots record the position of the probe-arm in terms of analog voltages. The Interface reads these voltages, displays them on the front control panel, and sends them to other parts of the controller circuitry. It also compares the feedback pot outputs to a predetermined set of range voltages. If one of these feedback voltages exceeds the range voltages, the Interface turns on a front panel out-of-range LED and shuts of the corresponding motor. This protects the Mechanical Assembly so that the motors won't try to move the probe-arm beyond its intended range of travel.

Besides watching the feedback potentiometers, the Interface also controls the two DC motors. Upon certain applied signals from either the manual switches located on the front control panel or from the Auto-Scanner circuitry, the Interface operates sensitive relays to turn on the motors, change their direction, or adjust their speed. The Interface contains special circuitry to control the inertial drift of the motors as well. When trying to halt them, the Interface not only cuts off the motor power, but it also sends each a short electrical pulse which briefly reverses the motor power. Otherwise, if a reverse pulse is not sent, the motors tend to turn a few extra revolutions due to the inertia of the gear heads. The length of this

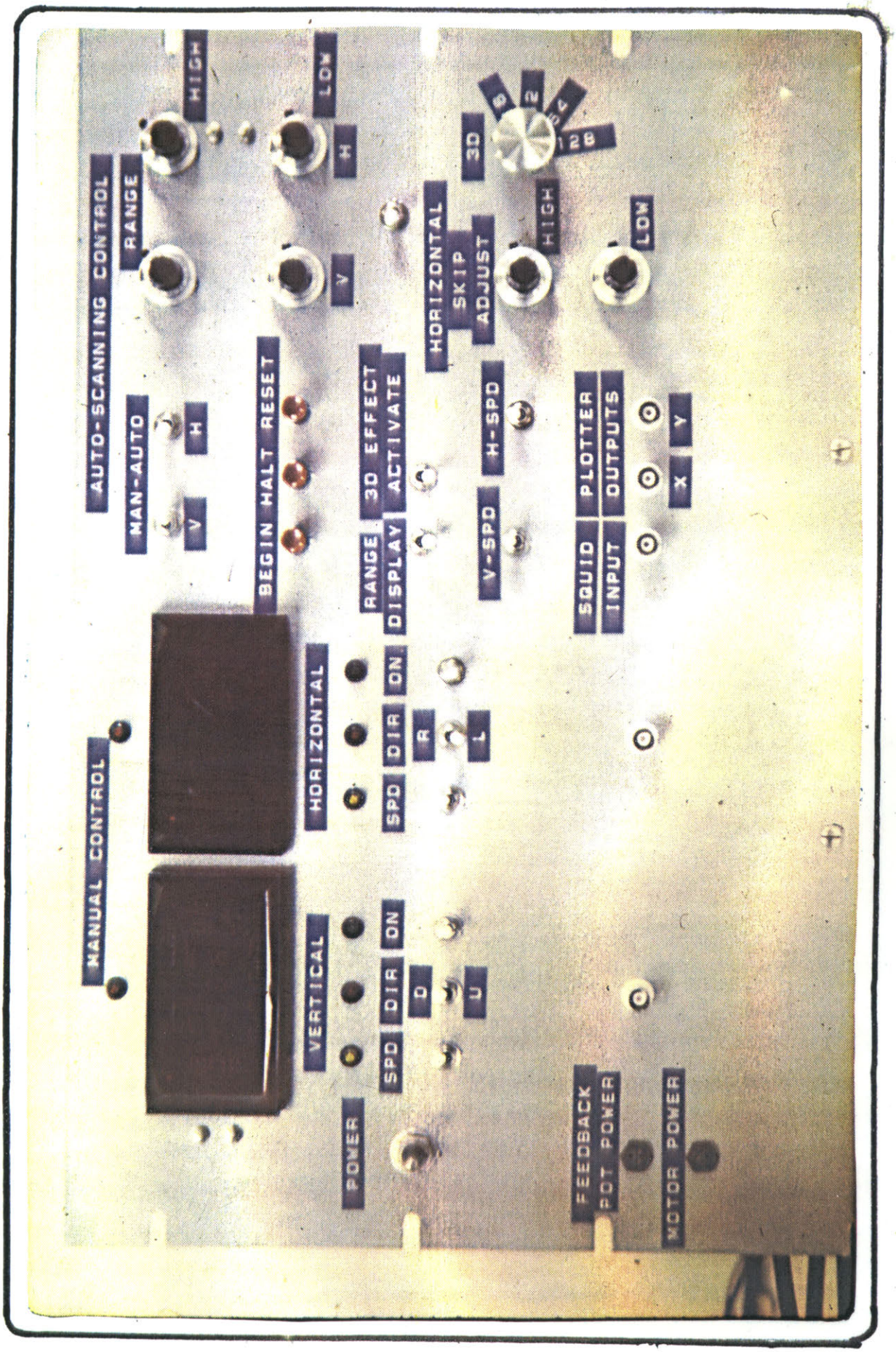
AUTO-SCANNING CONTROL
RANGE
HIGH
LOW
H
V
MAN-AUTO
H
V
BEGIN HALT RESET
RANGE
3D EFFECT
DISPLAY
ACTIVATE
HORIZONTAL
SKIP
ADJUST
3D
HIGH
LOW
V-SPD
H-SPD
SQUID
INPUT
PLOTTER
OUTPUTS
X
Y
MANUAL CONTROL
HORIZONTAL
SPD
DIR
ON
R
L
VERTICAL
SPD
DIR
ON
D
U
POWER
FEEDBACK
POT POWER
MOTOR POWER

FIGURE 12

reverse pulse is easily controllable so that it can be adjusted to just stop the motors without turning them in the opposite direction.

**Digital Auto-Scanning Mode**

The second part of the circuit is named the "Auto-Scanner". Its purpose, when started, is to be able to make a complete chip scan by pressing a few buttons. It causes the "vertical motor", controlling the vertical movement of the probe-arm, to begin sweeping the chip up and down over the probe. It also causes the "horizontal motor" to step the probe-arm a few thousandths of an inch, everytime the "vertical motor" reaches the end of its travel and reverses direction. Due to this raster pattern of movement, the entire surface of the chip is examined by the probe. Also, when the probe-arm reaches the end of its travel in the horizontal direction, the two motors are stopped and reset to their original starting position.

Four adjustable pots on the front panel allow one to set the four boundaries of the scan. Two are for the vertical direction and two are for the horizontal direction. If by chance, the motors failed to stop at one of the "bounding voltages" produced by these pots, the Interface circuitry would halt the offending motor at its own "range voltage" (described in the previous section) before any damage to the mechanical assembly occurred. In addition to the "boundary pots", there are three control buttons for the Auto-Scanner.

BEGIN-- initiates the scanning motion of the probe-arm

HALT-- immediately stops the motors

RESET-- returns the probe-arm to its starting position

Also, two other pots on the front panel control the length of the stepping pulse sent to the horizontal motor. There is one pot for each end of the vertical motor's travel. These pots basically determine the density of a scan across a chip by controlling the horizontal spacing of each vertical sweep.

The circuitry for the Auto-Scanner is primarily digital, utilizing simple combinational logic and flip-flops to implement the scanning function. The circuitry also includes timing chips for controlling the length of the stepping pulses sent to the horizontal motor.

**Output Signal to Plotter**

This part of the circuitry, referred to as the Formatter, outputs two analog voltages for use with an X-Y Plotter. It formats the two feedback pot outputs and the SQUID output such that the plotter appears to display a three-dimensional contour map of the areas on a chip where magnetic flux is trapped. The analog circuitry essentially adds the SQUID output voltage to the signal from the horizontal feedback pot. This drives one axis of the plotter. The signal from the vertical feedback pot drives the other axis. Hence, as the chip makes vertical sweeps over the probe, the plotter traces out the flux pattern seen by the probe. The result is many such traces, spaced closely together, representing the entire area of the chip.

The Formatter also adds two other special-effect signals to the vertical feedback pot output before sending it to the plotter. One is a mechanical backlash compensating signal. Backlash occurs when the vertical motor, sweeping the chip over the probe, reverses direction. It has the effect of moving the vertical feedback pot while leaving the probe-arm stationary for a very short distance until the vertical motor takes up the slack. The backlash control circuit adds in a small manually set voltage to the vertical feedback pot signal for the duration of the time the probe-arm sweeps backwards. This offsets the plotter trace obtained during backward sweeps such that it aligns with the signal obtained on forward sweeps.

The other special-effect signal is a 3D offset voltage, similar in nature to the backlash offset voltage. The difference is that the 3D offset is continually increasing by a fixed increment with each forward scan. Thus, each pair of traces plotted, consisting of a forward trace and a reverse trace, are misaligned by a constant distance from the previous pair. The result is that the final output of the plotter, after scanning over the complete surface of a chip,

now resembles the shape of a parallelogram instead of a square. The idea was to generate the appearance of a three-dimensional conformal map of the chip surface at the plotter output. As it turns out, the peaks and valleys associated with the presence of flux at the chip surface are not enough well-defined so that the eye can imagine a 3D map. Noise from the SQUID tends to obscure the flux patterns and confuse the eye. For that reason, we found it best, until the noise from the flux detection apparatus can be reduced, to leave out the 3D offset. This emphasizes the peaks and valleys so that they are more readily apparent to the eye. The circuitry for the 3D effect relies upon a simple binary counter and D/A Converter. The length of the offset can be adjusted by a dial on the front panel.

## FLUX DETECTION APPARATUS

This part describes our deliberations in designing and fabricating a flux magnetometer appropriate for detecting flux vortices. The basis of our magnetometer was an rf-SQUID manufactured by the S.H.E. Corporation. Even though the SQUID is a complete magnetometer by itself, it is not set up for detecting minute flux vortices. I had to find a method to couple flux from a vortex into the SQUID input coil using a small sense-coil. It was of utmost importance to design the sense-coil to make maximum utilization of the SQUID's inherent sensitivity. This meant maximizing the amount of flux transmitted from the sense-coil to the SQUID input coil. The small size of the sense-coil, dictated by our resolution requirements, complicated this task. I explored two paths towards resolving this problem. The first was to use a superconducting transformer between the sense-coil and SQUID input coil. The transformer would essentially optimize the flux transfer from the low-inductance sense-coil to the relatively high-inductance SQUID input coil. The second was to ignore inductance mismatches between the SQUID and sense-coil, and simply try to wind as many turns as possible in as dense a volume as possible. This second approach assumes that the coupling coefficient of the transformer will be poor enough that a direct connection will provide a greater signal to the SQUID. Our efforts in designing these two sense-coil systems will be discussed in the following sections. Experimental evaluation of these two systems will be discussed in Chapter IV.

### SQUID Magnetometer

The SQUID system, for our purposes, is an ultra-sensitive flux detecting device. It outputs an analog voltage corresponding to a flux change through its input coil. Since the SQUID input coil is already in place, one only has to attach a superconducting sense-coil to the leads of the input coil. A change in flux through the sense-coil will induce a persistent

current through the SQUID input coil which will generate a proportional output voltage. Thus, the SQUID can be thought of as a four terminal device with the output voltage expressed as a function of the input current. We used a S.H.E. Hybrid SQUID with a maximum sensitivity of:

$$\delta_I = 4.7\times10^{-11}\frac{A}{mV} \quad (\times 100 \text{ scale})$$

This means 47 pA of input current generated a 1mV output voltage.

The SQUID, however, exhibits white and 1/f noise which ultimately limits its sensitivity. Using a Tektronix Spectrum Analyzer, I measured the peak noise for a 1 Hz bandwidth. (1 Hz is the high-end cut-off filter I used most frequently when operating the flux scanner.)

$$V_N = 4.84 \times 10^{-4} \frac{V}{\sqrt{Hz}} \quad (\text{at } 1 \text{ Hz}, \times 100 \text{ scale})$$

Multiplying by the SQUID sensitivity to find the equivalent input current noise:

$$V_N\delta_I = I_N = 2.275\times10^{-11}\frac{A}{\sqrt{Hz}} \quad (\text{at } 1 \text{ Hz})$$

This shows the important result that the input current from a flux vortex to the SQUID must be at least 100 pA in order to have a signal to noise ratio of 4:1.

It is important to note here that I recorded these noise measurements under typical flux scanner operating conditions. I placed a 4-turn .009 inch I.D. sense-coil in the scanning position and lowered the entire flux scanner assembly into the shielded dewar. Although the size and positioning of the sense-coil would change by a small amount, this was not critical to the noise measurement.

**Sense-Coil**

The most important feature of a sense-coil is its flux transfer capability. The design must be optimized for maximum flux transport into the SQUID. This "optimal design" is readily

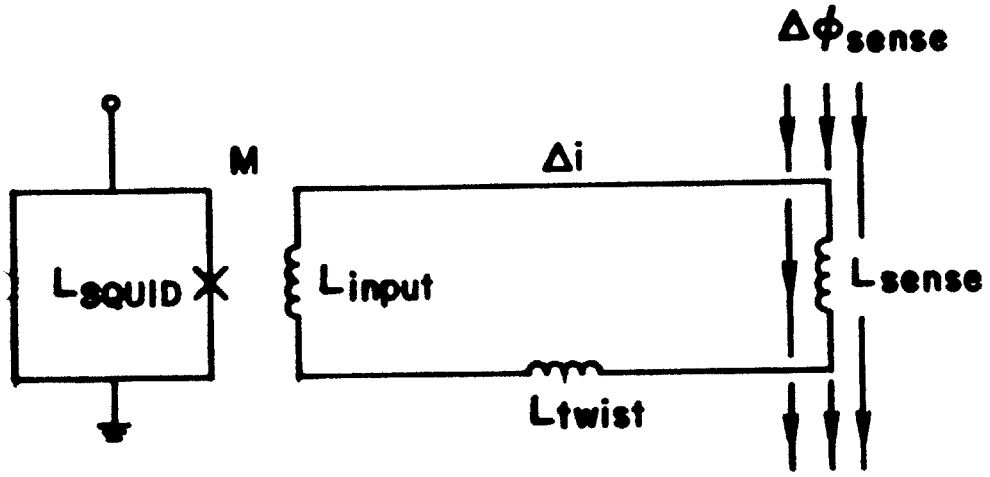


FIGURE 13

calculable. Consider the previous diagram (Figure 13). $L_{sense}$ is the sense-coil inductance. $L_{twist}$ is the self-inductance of the twisted pair of leads connecting the sense-coil to the SQUID input coil. For tightly twisted thin-gauge Niobium wire, this self-inductance is approximately $3\times10^{-9}$ H/cm [3]. $M$ represents the mutual inductance between the SQUID input coil and the SQUID itself:

$$M = k\sqrt{L_{squid}L_{input}}$$

where $k$ is the flux coupling factor between the two inductances.

$$0 < k < 1$$

The inductive circuit is a closed superconducting path. Lenz's Law requires that the sum-total of all flux though the closed path remain constant. Hence for a change in flux through the sense-coil, $\Delta\phi_{sense}$, there will be an induced current $\Delta i$ generating an equal amount of flux in the opposite direction. This phenomenon is written as:

$$\Delta i(L_{sense} + L_{twist} + L_{input}) = \Delta\phi_{sense}$$

We also know how to write the change in flux through the SQUID due to the induced persistent current $\Delta$i.

$$\Delta\phi_{squid} = M\Delta i$$

Solving for the flux input to the SQUID:

$$\Delta\phi_{squid} = \frac{k\sqrt{L_{squid}L_{input}}}{(L_{sense} + L_{twist} + L_{input})}\Delta\phi_{sense}$$

The three variables $k$, $L_{squid}$ and $L_{input}$ are fixed by the manufacturer of the SQUID. $L_{twist}$, is fixed by the distance the sense-coil is located from the SQUID. This distance is $\cong$ 18 inches, so $L_{twist} \cong 0.14\ \mu H$. That leaves only $L_{sense}$ and $\Delta\phi_{sense}$ as free variables. In order to maximize the above expression we want to make $\Delta\phi_{sense}/(L_{sense}+L_{twist}+L_{input})$ as large as

possible. Hence, the optimal sense-coil will have a low self-inductance, while still having the ability to couple in a large amount of flux from a vortex. Given the monopole field of a vortex, a small, low-inductance sense-coil can still couple in a large amount of vortex flux, if we can position it close to the thin film.

Another consideration is resolution requirements. We need to design a sense-coil which has a very small diameter so that it can distinguish between vortices trapped in closely-spaced holes in a thin film. A small diameter automatically means that the sense-coil inductance will be small compared to $L_{input}$. To couple in a large amount of flux, we can simply wrap the sense-coil with a large number of turns. If the sense-coil diameter is extremely small, the number of turns will not raise $L_{sense}$ to a point where it becomes comparable to $L_{input}$. To achieve this optimal resolution and flux-linkage at the same time, a small diameter solenoidal design is the obvious choice.

The height of the solenoid is only limited by practicality. At the point which the SQUID input current generated by the topmost loop becomes less than the SQUID equivalent current noise, adding additional turns to the solenoid has a greatly diminished effect. Since the vortex signal falls off as $1/R^2$, this happens after only a small number of turns. Generally, it occurs when a sense-coil's height becomes comparable to its diameter.

To calculate the self-inductance of this solenoidal sense-coil design, I used the following formula[4]. It assumes that the field at a particular point on the axis of the solenoid is constant over the entire cross-sectional area in which that point lies.

$$L = \frac{\mu_o N^2 A}{\sqrt{4R^2 + l^2}}$$

$\mu_o = 4\pi \times 10^{-9}$ H/cm
$N$ = number of turns on solenoid
$A$ = cross-sectional area of solenoid
$R$ = radius of solenoid
$l$ = length of solenoid
(Note: 2.54 cm = 1 inch)

This is only a fair approximation of the total self-inductance, but it gives ballpark numbers to work with. Given our minimum sense-coil diameter of .009 inches with .0025 inch diameter Nb wire, this formula provides values of 2-5 nH for the sense-coil inductance (3-7 stacked turns). Hence,

$$L_{sense} + L_{twist} << L_{input}$$

With this short solenoidal sense-coil design, we transfer maximum flux from a vortex into the SQUID due to the sense-coil's low inductance and its large flux linkage ability.

One improvement that can be made to this basic sense-coil design involves wrapping another layer of windings on top of the first. This increases the flux linkage through the coil while maintaining its relatively low inductance and fine resolution. The actual sense-coils used in flux scanner experiments followed this design. Typical specifications are shown below:

| | |
|---|---|
| Inner Diameter | .009 inches |
| # turns inner layer | 5 |
| # turns outer layer | 4 |
| Height | .0125 inches |
| Outer Diameter | .020 inches |
| Nb wire thickness | .0025 inches (including insulation) |

The key idea behind this double layer approach is to place a large number of turns near the chip surface where the vortex field is strongest.

We can calculate the inductance of this sense-coil design using the formula for a short solenoid presented earlier. Plugging in the above values:

$$L_{sense} \cong 4.2\ nH$$

We can also estimate the total flux it will couple through its turns when passing over a vortex. As shown earlier in the "Mechanical Assembly" section:

$$\Delta\phi_{loop} = \phi_o\left(1-\frac{d}{\sqrt{c^2 + d^2}}\right)$$

This formula holds for a single loop of radius $c$, parallel to the chip surface but spaced a distance $d$ away. Estimating $\Delta\phi_{total}$ for all 9 turns of our sense-coil:

$$\Delta\phi_{total} = \phi_o(9-0.59-0.71-0.79-0.84-0.88-0.90-0.92-0.94-0.95)$$

$$= 1.48\phi_o$$

From this we can calculate the signal-to-noise ratio at the SQUID output terminals.

$$\Delta i_{sense} = \frac{1.48\phi_0}{L_{sense} + L_{twist} + L_{input}} = 1.43\ nA$$

$$\text{where} \quad \phi_o = 2.07\times10^{-15}\ Wb$$

So, for a 1 Hz bandwidth,

$$\frac{\Delta i_{sense}}{I_N} = 63$$

Our measured signal-to-noise with the sense-coil stationary was actually about one-half of this, but it was still adequate for observation of individual vortices.

**Superconducting Transformer**

With a transformer one can theoretically improve the signal-to-noise between the sense-coil and SQUID by improving the flux transfer between the two unmatched inductances. Take for example the circuit diagram on the following page (Figure 14). One can write the following two equations:

$$\frac{\Delta\phi_s}{\Delta\phi_{sense}} = \frac{k_{t1}\sqrt{L_pL_s}}{L_p + L_{lead1} + L_{sense}}$$

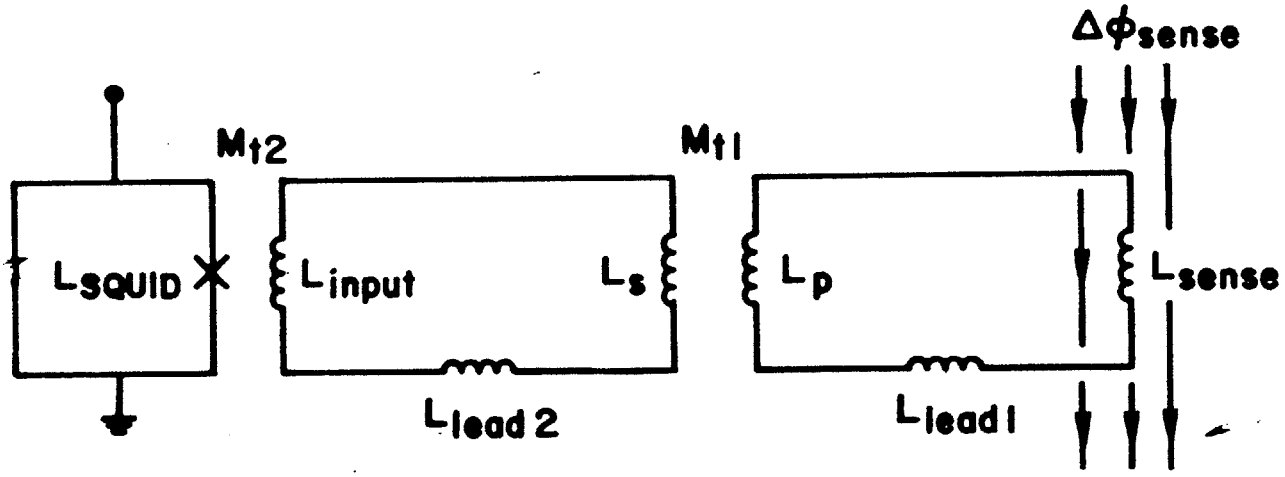


FIGURE 14

$$\frac{\Delta\phi_{squid}}{\Delta\phi_s} = \frac{k_{t2}\sqrt{L_{input}L_{squid}}}{L_{squid} + L_{lead2} + L_s}$$

Eliminating $\Delta\phi_s$, the flux change through the secondary coil of the transformer, the result is

$$\frac{\Delta\phi_{squid}}{\Delta\phi_{sense}} = \frac{k_{t1}k_{t2}\sqrt{L_{squid}L_{input}L_pL_s}}{(L_p + L_{lead1} + L_{sense})(L_{input} + L_{lead2} + L_s)}$$

Rearranging,

$$\frac{\Delta\phi_{squid}}{\Delta\phi_{sense}} = [k_{t1}k_{t2}\sqrt{L_{squid}L_{input}}]\left[\frac{\sqrt{L_p}}{L_p + L_{lead1} + L_{sense}}\right]\left[\frac{\sqrt{L_s}}{L_s + L_{input} + L_{lead2}}\right]$$

Differentiating the second and third terms with respect to $L_p$ and $L_s$ respectively, while holding all other variables constant, we find the values for $L_p$ and $L_s$ which maximize this expression:

$$\begin{aligned} L_s &= L_{input} + L_{lead2} \\ L_p &= L_{lead1} + L_{sense} \end{aligned}$$

We know

$$L_{input} >> L_{lead2}$$

So, the value for $L_s$ which maximizes the flux transfer is

$$L_s \cong L_{input}$$

Plugging into the above equation while assuming ideal coupling conditions, that is,

$$k_{t1} = k_{t2} = 1$$

we find,

$$\frac{\Delta\phi_{squid}}{\Delta\phi_{sense}} = \frac{\sqrt{L_{squid}L_p}}{2(L_p + L_{lead1} + L_{sense})}$$

In this expression, $L_p$, $L_{lead1}$, and $L_{sense}$, are the three variables we are free to adjust. Setting

$$L_p >> L_{lead1} + L_{sense}$$

we optimize our flux transfer. If we compare this expression with the previously obtained expression for $\Delta\phi_{squid}/\Delta\phi_{sense}$ in the section entitled "Sense-Coil", we see that the transformer gain can be written:

$$G_t \cong \frac{1}{2}\sqrt{\frac{L_{input}}{L_p}}$$

The smaller $L_p$ is, the better the gain. But if $L_p$ becomes too small, we exceed the condition where $L_p$ is much greater than $L_{lead1} + L_{sense}$. Writing the true gain,

$$G_t = \frac{k_{t1}}{2}\frac{\sqrt{L_{input}L_p}}{(L_p + L_{lead1} + L_{sense})}$$

we see that for $L_p = L_{lead1} + L_{sense}$, the gain is maximized. Since $L_p$ is typically on the order of a few nano-Henries and $L_{input} = 2\mu H$, the gain for this ideal transformer is on the order of 10. The only concern is the coupling factor, $k_{t1}$. If it is only 1/10, we've lost our advantage. The actual gain results from our hand-wound, shielded, solenoidal transformers will be discussed in Chapter IV.

Constructing these transformers was not a simple task due to their small size. In order to match the inductance of the sense-coil with a transformer primary of large diameter, I used a double turn primary. The inductance of a coil, with a radius much larger than the length, is given by the following expression[5]

$$L \cong \mu_o R N^2 \left[ \ln \frac{8R}{a} - 2 \right] \frac{H}{cm}$$

R = radius of loop (cm)
a = radius of wire (cm)
N = number of turns

Since

$$L_{lead1} \cong 6 \text{ nH (leads were 2 cm long)}$$
$$L_{sense} \cong 4.2 \text{ nH (calculated earlier)}$$

$L_p$ had to be about 10.2 nH. Since we used a double turn of .0025 inch diameter Nb wire, this implied a radius,

$$a_p = .031 \text{ inches}$$

Then, using a secondary which matched the inductance of the SQUID input coil plus the superconducting leads (2.14 $\mu$H total), I calculated the number of turns required. For the radius of the secondary, I used the outer radius of the primary,

$$a_s = .034 \text{ inches}$$

The number of turns came out to be approximately 25, so I configured it in 5 layers of 5 turns each. The layers were wound one over the other. The overriding concern in designing the coil form for the transformer was optimal coupling between the primary and secondary. For that reason, I chose to wind the secondary in layers so that it would match the geometry of the primary.

I also fabricated a Nb superconducting shield to pass over the transformer. It was cylindrical in shape with one end closed. This shielded the transformer from outside interference, so that the it wouldn't introduce any additional noise into the sense-coil's signal. As a general rule of thumb, for every diameter into the open end of the shield, the longitudinal field decays by a factor of 30. I placed the transformer two diameters deep into the shield which gave a shielding factor of 900. I ignored the transverse field since it points perpendicular to the axis of the transformer. Considering that the flux scanner is already in a low field environment, our shielding scheme was more than adequate.

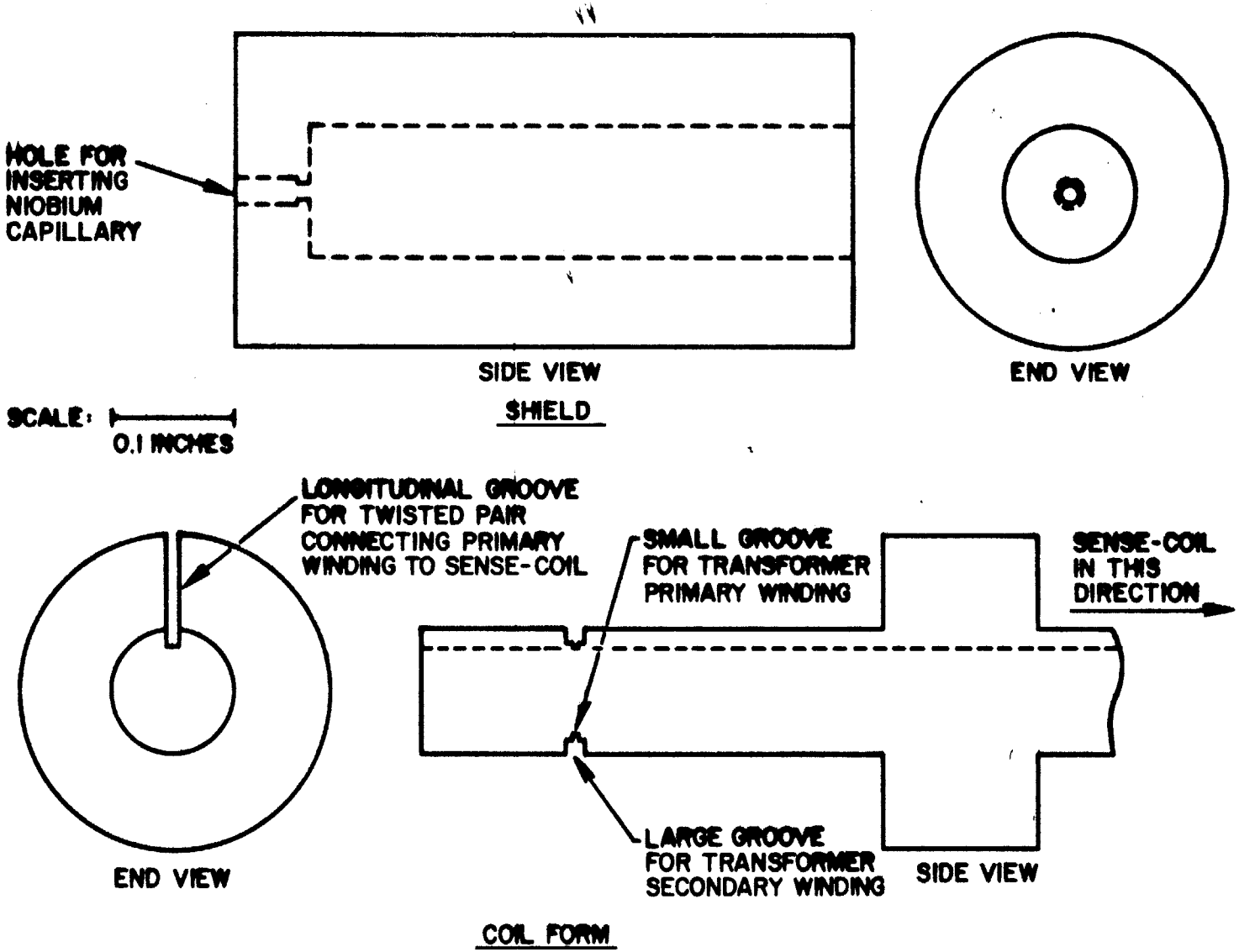
HOLE FOR
INSERTING
NIOBIUM
CAPILLARY
SIDE VIEW
END VIEW
SHIELD
SCALE:
0.1 INCHES
LONGITUDINAL GROOVE
FOR TWISTED PAIR
CONNECTING PRIMARY
WINDING TO SENSE-COIL
SMALL GROOVE
FOR TRANSFORMER
PRIMARY WINDING
SENSE-COIL
IN THIS
DIRECTION
END VIEW
LARGE GROOVE
FOR TRANSFORMER
SECONDARY WINDING
SIDE VIEW
COIL FORM

FIGURE 15

On the following page is a diagram of the coil form I used to wrap the transformer (Figure 15). The biggest hurdle I faced, in constructing this minute object, was connecting the primary to the sense-coil. The twisted leads from each had to be spot-welded together and then pushed into the groove cut along the length of the coil form. This was done with fine tweezers under a microscope, and a low-discharge spot-welder. Eventually the entire job was successfully completed and submitted to tests at LHe temperatures (See Chapter IV for the results).

## SHIELDING AND UNIFORM FIELD GENERATION

In order to account for all flux quanta present on a chip, the environmental magnetic field in the vicinity of the chip can not exceed 1$\mu$G. 1$\mu$G is just enough to populate 1 trapping site on the chip with 1 flux quantum. So, if the environmental field is shielded down to <1$\mu$G, no stray flux quanta can be trapped. (To calculate these figures, I divided $\phi_0 = 2.07 \times 10^{-7}$ G-cm$^2$ by the area of the hole array (.1875 inches)$^2$(2.54 cm/inch)$^2$ = 0.23 cm$^2$. This results in $\cong$1$\mu$G which is the field at which 1 flux quantum would be generated in the hole array as the chip was cooled through $T_c$.) Through the use of highly permeable ferromagnetic shields and three-dimensional nulling coils, we tried to achieve this sub-microgauss environmental field. A picture of our shielding apparatus, which is attached to the top of the dewar and hangs down into the helium reservoir, appears on the following page (Figure 16).

### Ferromagnetic Shields

We used two cylindrical shields, each having one open end, to ensure a low-gradient, highly stable field in the vicinity of the probe and chip in the flux scanner assembly. Relying upon S. Bermon's knowledge of ferromagnetic shielding systems, we knew beforehand that our two shield system would only reduce the absolute field by a factor of around 10,000. Since the earth's field in our lab ranges around 300 mG, this would put the absolute field inside the shields at $\cong$ 30 $\mu$G which is much greater than our maximum allowable field of 1 $\mu$G. So, we concentrated on reducing field gradients and optimizing field stability inside the shields. They had to be below 1$\mu$G across the area of the chip in order to ensure no stray flux quanta would be generated when cooling through $T_c$. If the absolute field was above 1$\mu$G, it could always be nulled with our three-dimensional nulling coils.

The outer shield was installed just outside the dewar vacuum jacket when it was built. Judging from the dewar size, this shield is approximately 36" tall with a 17" diameter. The

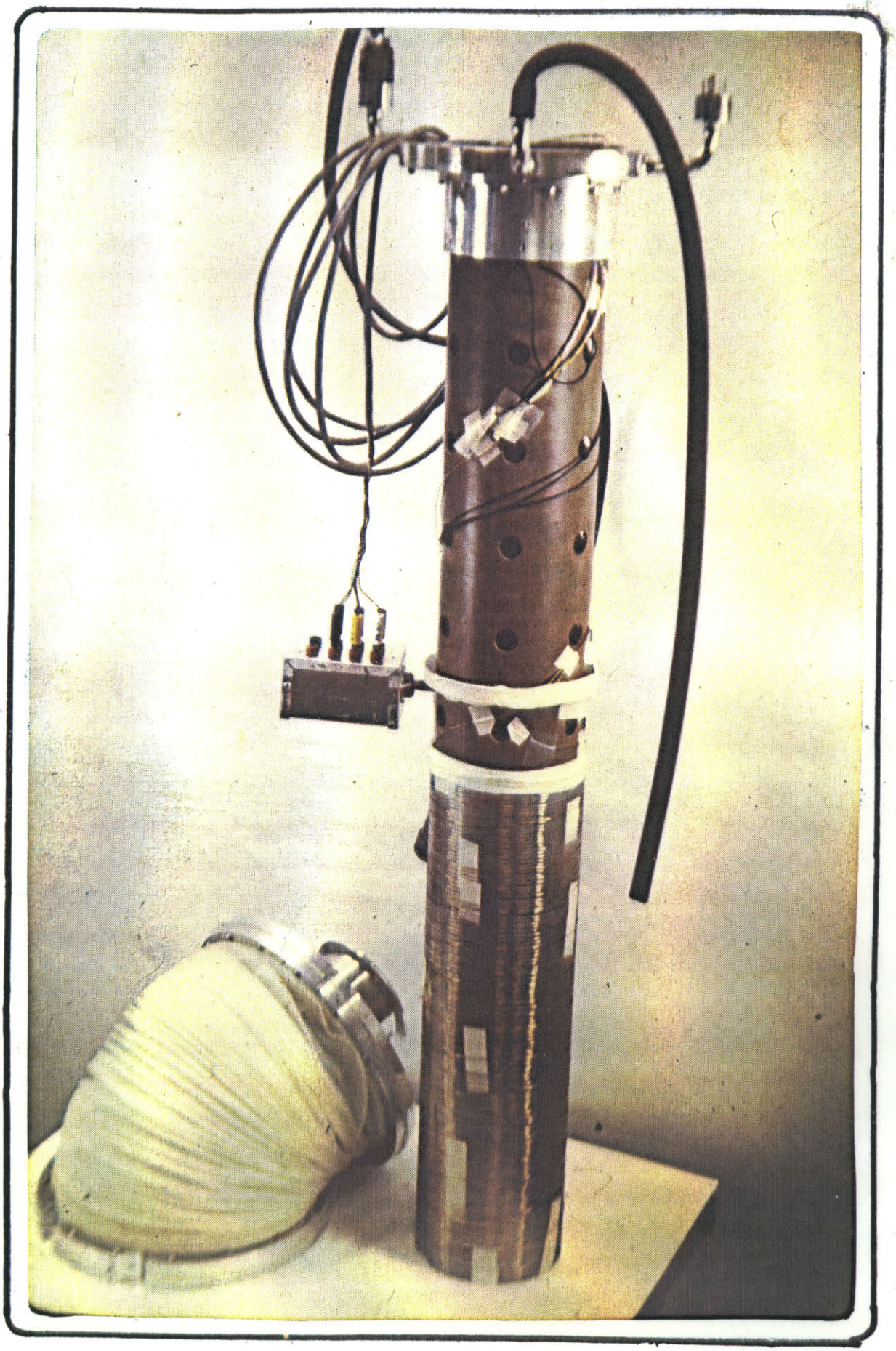

FIGURE 16

inner shield is a low-temperature shield[6], meaning that it is meant to be immersed in the helium reservoir. At 4.2 °K its permeability is a maximum. This shield has a 5.25" O.D. and is 17.75" high. It is suspended around a 5" O.D. phenolic tube which hangs down from the top of the dewar. Phenolic has a relatively low thermal conductivity, so this kept the boil-off rate to a minimum. Since the helium reservoir is 22.25" high for the dewar we used, and the inner shield hung 3/4" above the reservoir bottom, the inner shield almost extended the entire height of the reservoir. When the flux scanner was lowered into the dewar, the bottom of the glass tube came to rest about 1" from the inner shield bottom. This placed the probe and chip about 3.5" from the inner shield bottom. According to measurements recorded by S. Bermon, the optimal positioning inside a shield, where the gradients are lowest and the shielding factor is greatest, happens to be about one diameter above the bottom. Because of our space restrictions, we did not have the exact optimal positioning, instead being 2/3 of a diameter away from the bottom of the shield.

We conducted our measurements of the field inside the shielding system with two devices. The first was a flux gate magnetometer manufactured by Hewlett-Packard. With this I took room temperature measurements outside of the dewar to determine the environmental field, and then compared these with measurements taken inside the cold dewar at the chip position. In tandem with these measurements, I degaussed both shields with a solenoidal coil wrapped around the dewar. (The coil had 8 turns per inch of vertical height with an 18" I.D.) Degaussing consists of applying a slowly decaying alternating current to the solenoidal coil. This has the effect of re-orienting the magnetic dipoles inside the molypermaloy material so that they tend to cancel remanent fields within the shielded area. My optimal degaussing current began with 1/2 Amp at 8 Hz and decayed to a few microamps. I found from the flux gate measurements that the differential transverse shielding factor was 2400. The remanent field after degaussing was 130$\mu$G.

The other more precise field measurement device, I used, was the SQUID magnetometer. The SQUID can only be used at LHE temperatures, but it can measure fields down to a few microgauss reliably. It was mounted on a three-coordinate (X-Y-Z) positioning rack which could be accurately moved within $\pm 1/16$ of an inch. Thus, with this device, we could accurately measure field gradients and field stability. Due to the construction of the flux scanner mechanical assembly, the chip plane was parallel to the shields' common axis. Hence we measured the field gradients by orienting the SQUID loop within the plane of the chip and moving it both horizontally and vertically within this chip plane. The result was a vertical field gradient of $1.5\mu G/0.25$ inch and a horizontal field gradient of $2.25\mu G/0.25$ inch. (0.25 inch is the length of each edge of the chip.) Although these numbers did not meet our goal of $<1\mu G/0.25$ inch, they were certainly good enough to warrant using this shielding scheme for initial experimentation. At worst these results dictate no more than 2-3 flux quanta unaccounted for. The field stability was 0.125 $\mu$G/day as long as no large magnetized metal objects were moved around the lab. This value was well below our requirements.

**Nulling and Field Generation Coils**

To bias the remanent field inside the dewar so that it was zeroed at the chip position, I used three coils mounted perpendicular to each other. To mount these coils, we machined small grooves into the phenolic cylinder supporting the low temperature shield. To generate fields transverse to the shields' axis, I used two single turn saddle coils placed perpendicular to one another. A Helmholtz coil generated a longitudinal field. Using the SQUID magnetometer, I nulled the field with respect to the center of the chip position in each of these three coil directions. I was able to null accurately down to about $1\mu G$. To produce the nulling currents, I employed batteries because of their low-noise, stable output.

Next, to account for remanent fields produced by the flux scanner mechanical assembly inside the shields, I nulled again using the flip-coil described earlier in this chapter. The

flip-coil allowed me to null the transverse field only, because the coil rotates about an axis parallel to the shields' axis. But this was the most important direction in which to accurately null the remanent field anyways, because this is the only direction in which the chip traps flux. Because of earlier measurements taken of the flux scanner's remanent field in another shielding system, we knew that the field gradients at the chip position due to the apparatus did not exceed several microgauss per inch[7]. However, we were not assured that the absolute field was under 1 $\mu$G. With the flip-coil, we were able to successfully null this absolute field down to several microgauss. Fortunately, the flip-coil could null more accurately than the S.H.E. SQUID magnetometer. The inductance of its coil matched the input loop to its SQUID almost exactly, providing maximum sensitivity. (The sensitivity of the S.H.E. SQUID magnetometer was purposely reduced so that fields on the order of several gauss could by measured without exceeding the high-field cut-off range of a SQUID.)

The final piece of the shielding system was a rotatable saddle coil which fit inside the large phenolic tube holding the low-temperature shield. This coil was mounted on a smaller phenolic tube with a rim glued on at the top. The rim rested on six nylon bolts screwed in from the outside of the large tube. With strings extending up to the top of the dewar, one could rotate this coil until it was in a position to generate a field perpendicular to the chip surface. This coil was used mainly to generate absolute fields for flux-trapping trials. That is, it would produce finely controlled ambient fields to cause flux quanta to be trapped in a chip as it was cooled through $T_c$. I calibrated this coil using the S.H.E. SQUID magnetometer.

## TEST CHIPS

For the purposes of this thesis, we decided that a "coarse" array of pinholes through a superconducting thin-film would be best. First, we wouldn't have to struggle beyond our already established method of wrapping sense-coils to meet resolution requirements. Secondly, a coarse array gave us enough room to make large pinholes. Large pinholes ensured that several flux quanta would be trapped at these sites before interstitial sites became populated. (To calculate this, we used work done by J. Clem for I.B.M. Research.) Together, these two criterion governed the layout of our first chip. It was an $8 \times 8$ array of .0045 inch squares spaced .025 inches apart. The thin-film was Niobium, 2500 Å thick. For further experimentation, we also made another chip with a denser $15 \times 15$ array of .003 inch squares spaced .0125 inches apart.

As the experiments proceeded, we found that the $8 \times 8$ array chip gave us the proper resolution for the .009 inch I.D. sense-coil. The peaks of vortices trapped in adjacent holes were easily distinguishable. Also, the incidence of vortices trapped in interstitial sites (i.e. between holes where potential energy wells may exist due to intrinsic film defects or due to the repulsive force of vortices already trapped in the array) proved to be minimal. Evidently the .0045 inch square holes were large enough to guarantee all fluxoids would fall into them.

## NOTES

1. S.H.E. Corporation, Cryogenic Instruments and Systems, 4174 Sorrento Valley Blvd. San Diego, CA 92121

2. B. Cabrera, "Remanent Magnetization of Cryogenic Construction Materials", Stanford University, Stanford, CA, 1977 (to be published).

3. R. P. Giffard, R. A. Webb, and J. C. Wheatley, Journal of Low Temperature Physics, **6**, (1972) pp. 533

4. J. D. Kraus and K. R. Carver, Electromagnetics, McGraw-Hill (1973) pp. 157.

5. F. W. Grover, Inductance Calculations Working Formulas and Tables, Dover Publications (1962), Chapter 16.

6. Cryoperm 10 material, Vacuumschmelze GMBH, West Germany.

7. When we measured the flux scanner's remanent field, the aluminum probe-arm and probe mount table were unattached. We were counting on the purity of the aluminum and cleanliness of the parts to introduce no additional field.

# CHAPTER IV: OBSERVATION OF TRAPPED VORTICES IN THIN FILMS

## CALIBRATION AND INITIAL EXPERIMENTS

Before attempting to scan a chip, I first assembled the flux scanner and tested the sense-coil and transformer by scanning over the fiducial lines. This section discusses the results of these initial experiments, especially those that led to improvements in the flux detection apparatus.

### Mobile Sense-Coil

In the original flux scanner design, the chip was stationary, while the sense-coil and transformer were mobile. This was done in the interest of being able to make electrical connections to chip pads in future experiments. However, this approach complicated the design of the flux detection apparatus. To connect the mobile transformer to the stationary SQUID, I used two superconducting capillaries: one was pliable Lead (10" long), and the other was relatively stiff Niobium (also 10" long). These capillaries shielded the twisted pair of superconducting leads connecting the transformer to the SQUID terminals. The stiff Nb capillary ran along the length of the probe-arm, while the pliable Pb capillary was bent into a "w" shape. As the probe-arm moved over its range of 0.375 square inches, the Lead capillary acted like an accordion.

Surprisingly, the transformer and sense-coil worked the first time upon immersion in the dewar. A successful scan was made across the fiducial lines recording a visible signal. The current passing through the fiducial lines in this test run was 5 $\mu$A, calculated to produce a flux in the sense-coil on the order of what a single flux quantum trapped in a chip would

generate. Yet one snag was encountered in this preliminary experiment. With disturbing regularity, the signal from the fiducial lines was suppressed on downward scans, while not on upward scans. Upon turning up the fiducial line current, this suppression was found to be constant and did not scale with the fiducial line current. This indicates that the suppression of the signal on downward scans was due to a constant, compensating, stray signal. My postulate was that it was due to the twisted pair moving inside the Lead capillary. If the capillary had trapped flux near a small separation between the twisted wires, and the wires moved through the field produced by one or several flux vortices penetrating the capillary, an inductive current comparable to that induced by the fiducial lines in the sense-coil could certainly be generated. It's very easy for the twisted leads to shift position inside the Lead capillary, as the probe-arm moves and flexes it.

Thus, I made the decision to switch the position of the probe and chip. This involved redesigning the chip support table and the probe arm. After completing these alterations, the improvement in the SQUID output signal upon scanning over the fiducial lines was remarkable. The trace was very clean. It didn't have any unknown stray perturbations as before.

**Transformer Results and Sense-Coil Upgrade**

Originally, the rationale behind constructing a transformer was to boost the signal generated by the sense-coil passing over a vortex. I was unsure whether the signal-to-noise ratio from using just a sense-coil would be adequate for observation of single flux quanta. So, I built the transformer with the intention of measuring its gain, and deciding whether its inclusion was necessary.

In order to make an accurate measurement of the transformer gain, two identical sense-coils were required. One sense-coil would be attached to the transformer primary and the other would be used as the "control". Because of the difficulty in winding the two sense-coils, they were only similar in the number of turns and inner diameter. The tightness of the

windings were not identical due to the difficulty in glueing the springy Nb wire. With these slightly imprecise sense-coils, I found the overall transformer gain to be no better than 2.47. Ideally it should have been on the order of 10, so this means the coupling factor $k_{11}$ was about 0.25. This is not an unreasonable number, although I expected it to be better.

It turned out that the signal-to-noise ratio for the 9 turn, .009 inch I.D. sense-coil alone, was about 25. This was calculated by comparing an observed vortex peak with the intrisic SQUID noise. This This signal-to-noise was high enough so that the additional transformer gain of 2.5 was not necessary. Instead of the transformer, I concentrated on building more sensitive sense-coils, while maintaining adequate resolution for the 8×8 hole array. I especially worked on the glueing technique for holding the 9 turn coils together. The goal was to achieve a tightly wound coil without allowing too much glue to accumulate between the individual turns. If this happened the flux sensitivity would degrade because the turns would be spaced further away from the chip surface. For the glue, I used GE Varnish diluted with alcohol. It stood up to thermal cycling which was always a concern.

The double layer sense-coils turned out to be very advantageous. Their inner diameter determines the effective resolution of the coil, so adding additional turns on top of the first layer did not diminish their accuracy. Because of the Meissner effect, all flux emanating from the chip surface between the I.D. and the O.D. of such a coil, finds it energetically favorable to pass outside of the coil. It is easier for the field lines to bend outside of the coil, than bend to the inside and then bend upwards through the coil. This postulate agrees with my experimental observations. The vortex peaks recorded by double-layer coils had the same width as those recorded by single-layer coils, but the overall height was greater.

Basically there was a two month shake-out period when I first began operating the flux scanner. It took that long to work out the major bugs described above, and get on the air with actual chips.

## SCANS ACROSS HOLE ARRAYS

All the scans completed up to this point in time have been done on the 8×8 array chip. The density of this array is the most optimal for use with the 9-turn .009 inch I.D. sense-coil. Also, almost all the scans shown on the following pages are single sweeps across a single row of the array. Because the complete 8 row scans tended to give a muddled picture, and because certain problems developed with the mechanical apparatus, it soon became obvious that single row scans were best to begin with.

The procedure I followed when preparing the flux scanner for an experiment was extensive. I first had to ensure that the sense-coil was properly spaced from the chip, and that this spacing was maintained as the chip moved in a plane over the sense-coil. Then I positioned the sense-coil over one of the rows in the array. I recorded the x-y coordinates from the panel display for each hole in that particular row. After that, I evacuated the glass tube containing the mechanical assembly. This I'd usually do overnight, immersing the flux scanner in the helium dewar the following morning. Cool-down took several hours on average because of the massive mechanical assembly. Then, if the Squid and sense-coil were operating properly, I'd "detrap" the chip with the heater. "Detrapping" consisted of heating the chip above $T_c$ to rid it of excessive flux captured in the relatively high field region of the dewar neck where the chip first passed through $T_c$. When detrapping the chip of this excessive flux, the ambient field inside the shielding system was always enough to ensure partial population of the holes in the chip. On this basis, I conducted most of the experiments. In these initial experiments, I never used the nulling coils because they had no visible effect on the hole population. (Reasons for this will be discussed in Chapter V.)

**Holes Populated By Single and Double Flux Quanta**

Upon completing the first successful scan, my first impulse was to verify that the peak signal received from a vortex agreed with earlier calculations. In the previous section, entitled "Flux Detection Apparatus", we determined that the peak $\Delta\phi$ through the 9 turn, .009 inch diameter sense-coil, generated by passing directly over a vortex, was $\sim 1.5\phi_0$ Using the equation

$$V_{peak} = \frac{\Delta\phi}{L\delta_I}$$

where $V_{peak}$ is the peak output voltage from the SQUID

$L$ is the inductance of the closed superconducting loop ($\cong 2\mu H$)

$\delta_I$ is the current sensitivity of the SQUID ($\cong 4.7 \times 10^{-8}$A/V)

one finds for the above values that $V_{peak} \cong$ 33mV. This result corresponds closely to our experimental results, especially considering our imprecise methods of measuring the chip to probe spacing and the diameters of the sense coil loops. The following two figures show typical scans (Figures 17 and 18). The peak values for the observed vortices range from 22mV to 37mV. These experimental values are certainly comparable to the $V_{peak} \cong$ 33mV calculated above.

Also, the spacing between vortex peaks agrees with my room temperature observation made before cool-down. I observed that the spacing between adjacent holes in the array was about 1V $\pm$10% on the front panel display. All the plots shown have a 1V per 10 divisions x-axis calibration. This means the vortex peaks should be spaced by 10 $\pm$ 1 divisions in the x-direction. This is certainly the case. All the peaks tend to be uniformly spaced, which tends to show they were vortices trapped in the hole array.

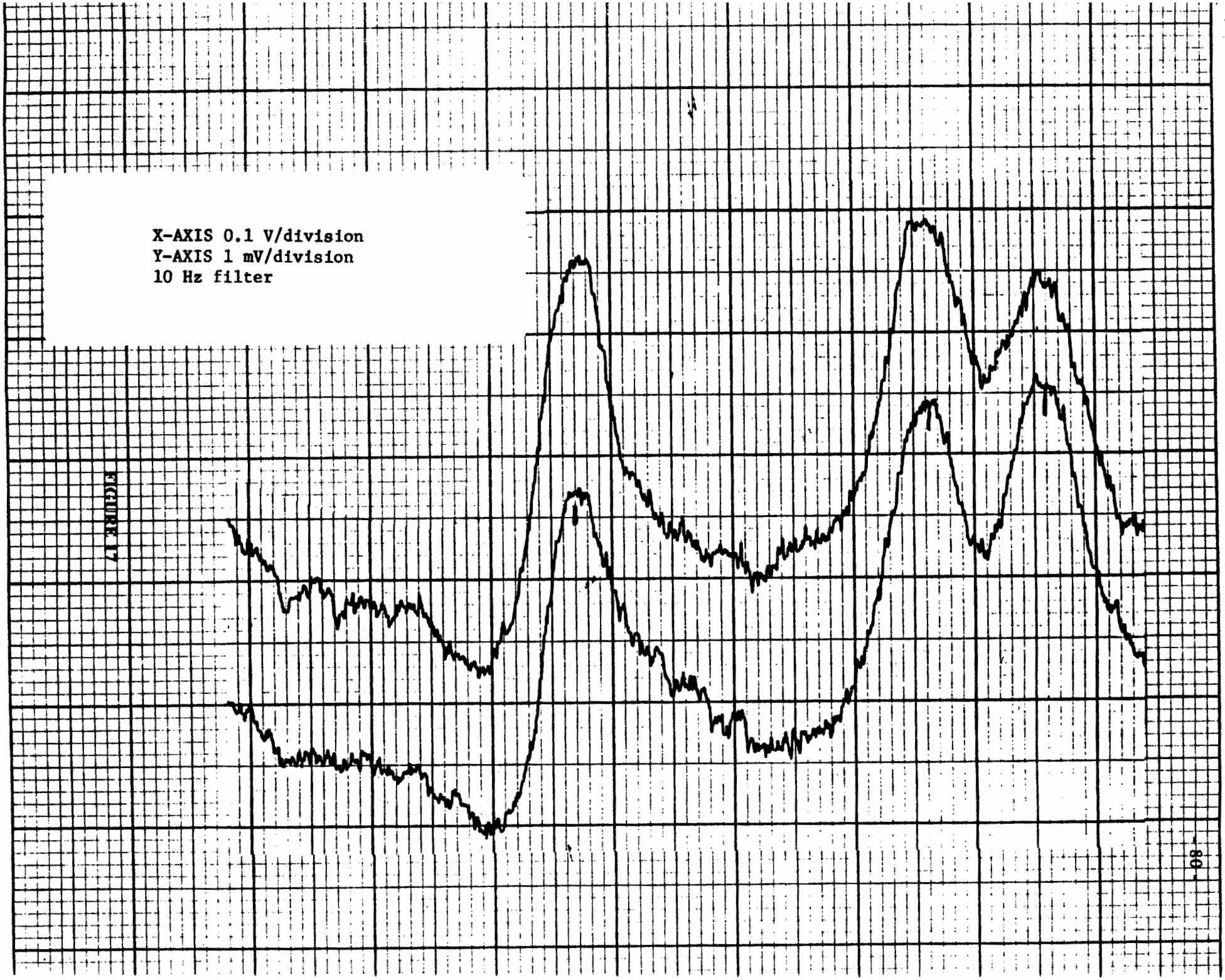


FIGURE 17

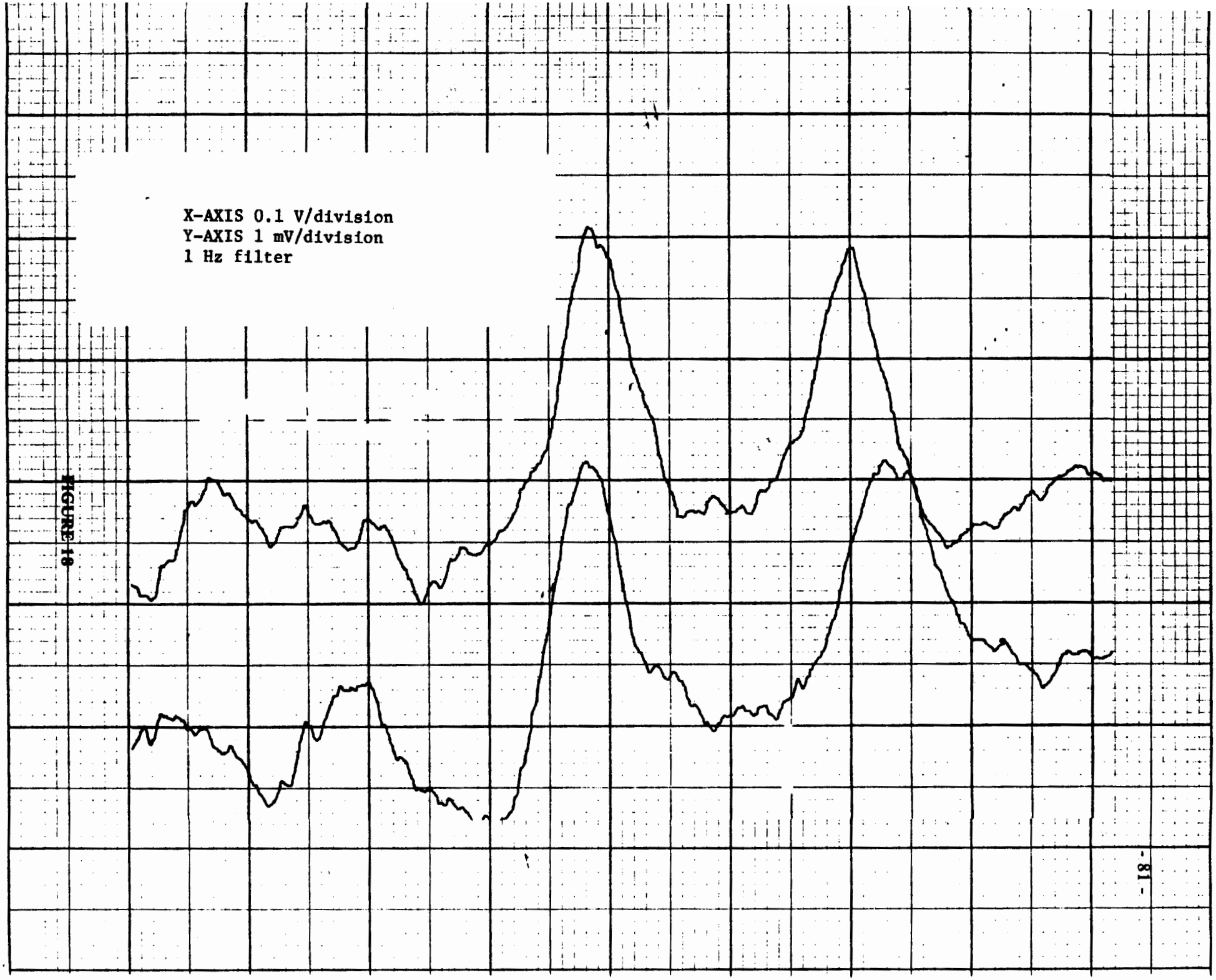


FIGURE 18

Note too that I made two successive scans in each figure across the same row. This was to ensure that the sharp peaks we observed in each figure were indeed due to flux passing through the sense-coil at that particular position, and not due to random SQUID fluctuations. Each set of successive traces do not exactly match for reasons yet to be explored. One possible explanation takes the temperature sensitivity of the SQUID into account. Any large amount of heat produced by friction in moving parts has an observed effect upon the SQUID output. While the flux scanner operates, it is probable that the gnashing gears and sliding probe arm produce non-uniform heat waves which affect the SQUID output in a non-uniform way. At this time, this appears to be the most reasonable explanation for why two scans taken under identical conditions don't match perfectly.

Another interesting observation concerns the repeatable, randomly-shaped bumps and dips in the baseline of each scan in each figure. These deviations do not have the symmetry of a vortex, and they tend to obscure the lower part of the vortex-induced peaks. One postulate is that these repeatable fluctuations in the baseline are due to the ambient field about the chip. With this idea in mind, it is instructive to examine Figure 19 which shows the SQUID drift and SQUID noise while the chip was motionless. One scan was taken with a 10 Hz filter and the other with a 1 Hz filter. The total time elapsed for each trace is equivalent to the time required for a single row scan. From this, it is obvious that the SQUID response is quite stable and predictable given a stationary chip. However, ambient fields associated with moving parts tend to introduce flux changes through the sense-coil. Even though the flux scanner assembly was made with non-magnetizable materials and cleaned, it is highly probable that magnetic impurities within the bulk Al and stainless steel still exist. This could possibly account for the unsteady but repeatable baseline.

Figure 20 shows an example of the unsteady baseline. All three traces were taken across a single row under identical conditions. In each trace the center vortex peak appears to be higher than the peaks to either side. This suggests that the baseline is humped in the center,

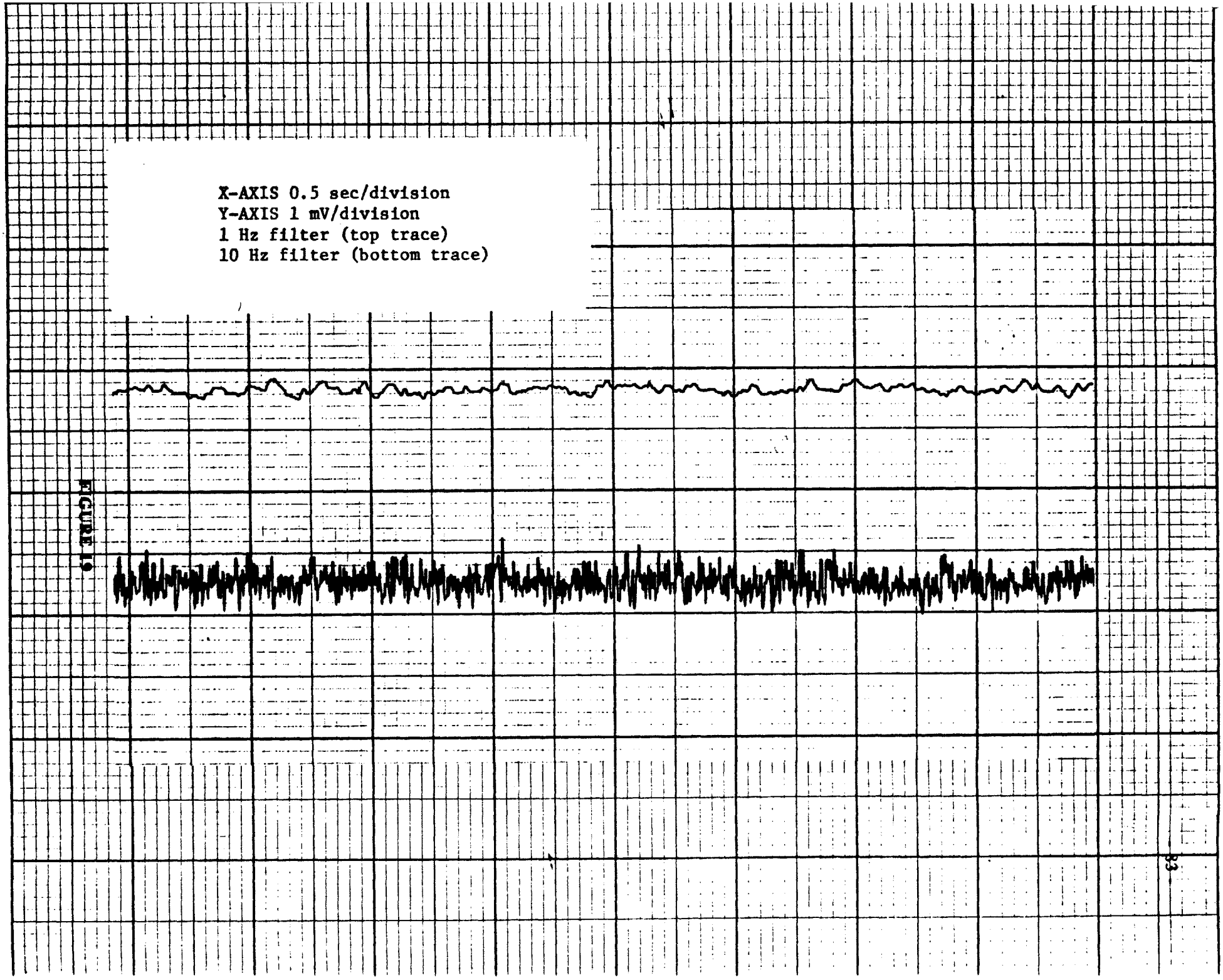
X-AXIS 0.5 sec/division
Y-AXIS 1 mV/division
1 Hz filter (top trace)
10 Hz filter (bottom trace)

FIGURE 19

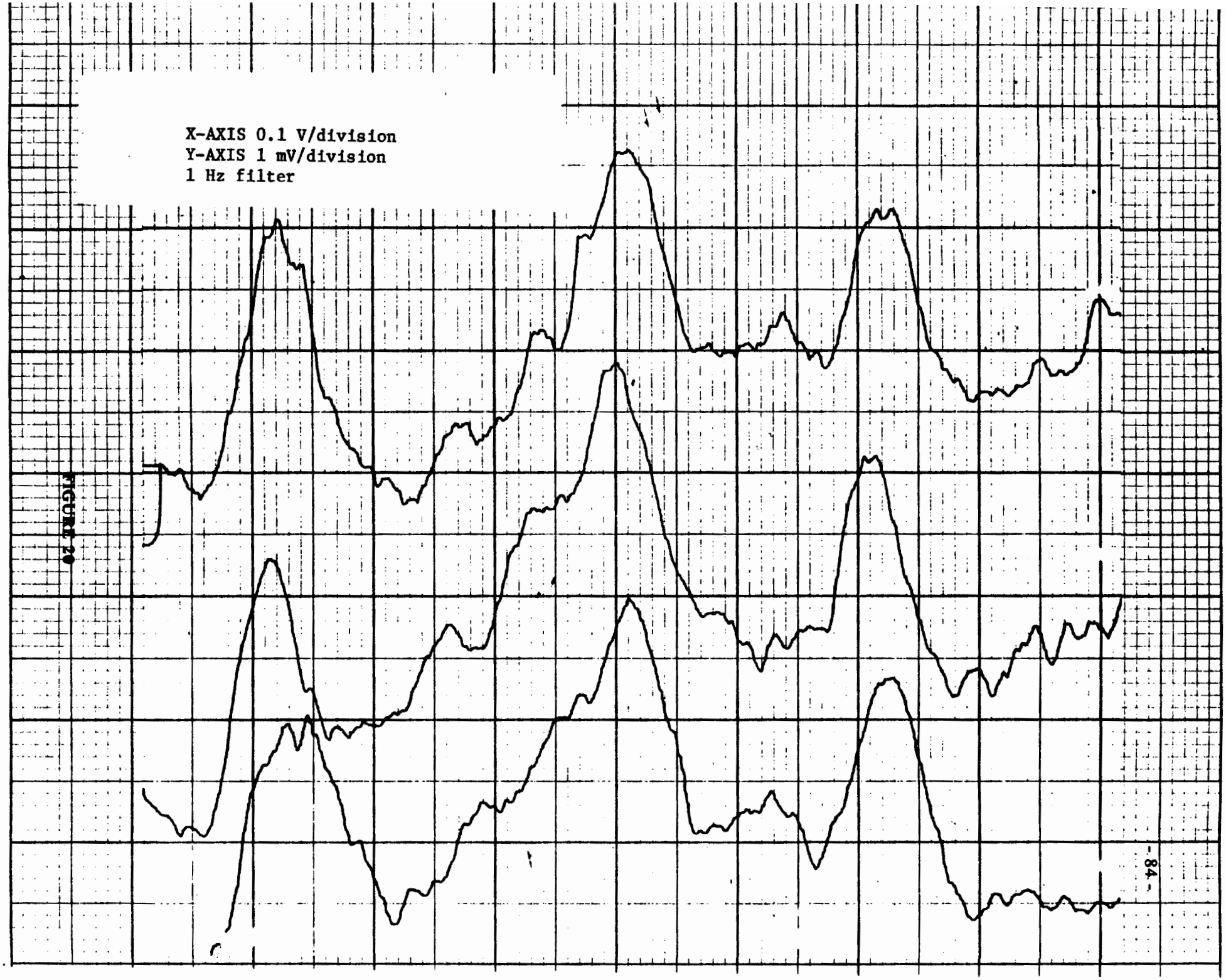


FIGURE 20

falling off to either side. As explained above, it is reasonable to assume that this is due to ambient fields which change with the movement of the mechanical assembly. The other non-repeatable variations in the baseline are most likely due to frictional heating of the SQUID as discussed earlier. (Also note that it is not appropriate to expect the baselines of different figures to match. These different scans were made on different rows during separate experiments.)

The plot on the next page (Figure 21) is one of several in which we observed the presence of doubly occupied holes in a chip. This always occurred when the chip was at least half populated with flux vortices. The more vortices trapped, the higher the probablility that it will become energetically favorable for two vortices to occupy a single hole. As shown by our calculations, the peak voltage generated at the output terminals of the SQUID will vary proportionally with the number of vortices trapped in a single hole. This is born out by the fact that the taller peak is about twice as high as the one alongside it. The reason for the progressive decline in the three single vortex peaks is probably due to the fact that the sense-coil crossed the row at a slight diagonal. In other words, the flux input to the sense-coil decayed as the row on the chip strayed from a direct path over the sense-coil.

**Signal-to-Noise**

One measure of the flux scanner's performance is the signal-to-noise associated with its scans across the 8×8 hole array. Comparing Figures 17 and 18 with Figure 19, one can make the following observation. The signal-to-noise ratio for a trace taken with the 10Hz cut-off filter is about 10 to 1. For a trace taken with the 1 Hz cut-off filter, it is about 25 to 1. These results assume that the noise is composed of the intrinsic SQUID noise plus environmental field fluctuations which change the flux through the sense-coil. I measured this noise by taking a time-based trace of the SQUID response with the chip stationary.

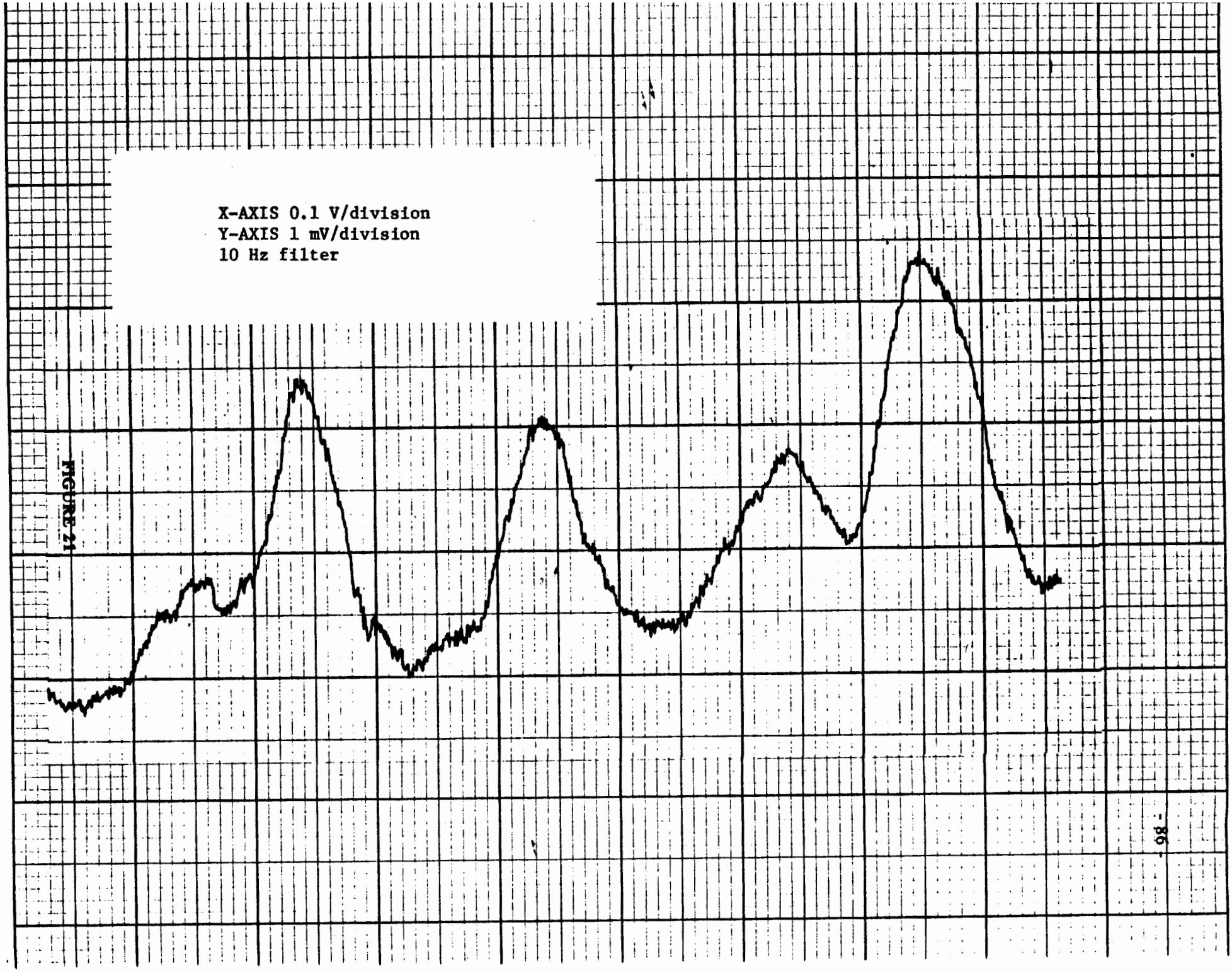


FIGURE 21

However, this method of calculating the signal-to-noise ratio is not a true measure of the flux scanner's performance. It doesn't take into account uncontrolled fluctuations in the SQUID response when the chip is moving. These unpredictable fluctations might beproduced by mechanical vibrations causing variations in the sense-coil to chip spacing, or they might be due to non-uniform heating of the SQUID as a result of mechanical friction. In light of these additional noise sources generated by the moving probe arm, there is a better measure of the flux scanner's true signal-to-noise ratio. This involves examining actual plots of scans across single rows of the 8×8 hole array. By determining how many times smaller one can reduce a vortex induced peak before it is indistinguishable form the background fluctuations, one arrives at an accurate measure of the flux scanner's performance.

Looking once again at Figures 18 and 19, it appears that for both figures, the background fluctuations are about one fifth the height of a vortex induced peak. It appears not to matter whether the 1Hz or 10Hz cut-off filter is in operation. The random fluctuations present with the moving sense-coil exceed the intrinsic SQUID noise.

**Resolution**

Another important measure of the flux scanner's performance is the minimum spacing between vortex peaks at which the flux scanner can tell them apart. This is how I defined the "resolution" of the flux scanner. Because flux is additive, vortices obey the law of superposition. As two vortices are brought more closely together, their tails add together, rapidly decreasing the dip between their peaks. The point, at which this dip becomes inseparable from background noise, is termed "the minimum resolvable distance". Using Figures 18 and 19, the minimum spacing between individual vortex peaks at which they'd become indistinguishable, appears to be approximately 6 divisions. Since 1 division represents 0.0025 inches, the minimum resolvable distance is 0.015 inches.

Of course, 0.015 inches is not the absolute minimum spacing between vortices in a thin-film at which one could observe them. Using signal decompositon techniques or data reduction, one could probably ascertain from the area under a large hump, just how many vortices it represented. This is one possible avenue by which finer hole structures in a thin-film could be observed without improving the sense-coil resolution.

**Repeated Flux Trapping Trials**

One of the basic intended functions of the flux scanner was to gather data on preferential flux trapping between two different hole sizes in a thin-film array. J. Clem and S. Bermon[1] have proposed a model for preferential flux trapping between two different potential energy wells, so experimental verification of the theory would certainly be valuable. Towards this end, the flux scanner must operate reliably. The ability to make many repeated scans of an entire chip is essential. One will be able to determine accurate probabilities of preferential flux trapping only by collecting a large amount of data.

The basic procedure of a single flux trapping trial is to heat a chip, and then cool it through $T_c$ in the presence of a known ambient field. After completing a chip scan, recording the position of all trapped vortices, the procedure would start over again. Implicit in this procedure, is the ability to accurately control the effective field from all sources, and thus, the number of flux quanta trapped in a chip. To date, this has not been accomplished. It is revealing, however, to study the limited attempts made with the flux scanner to control the ambient field around a chip. It's been observed that heating a chip disturbs the field which complicates any attempts to accurately control it [2].

In Chapter III, we discussed "Shielding and Uniform Field Generation". I set up the shielding system used in the following experiments just as described. Then, using a Flux Gate manufactured by Hewlett-Packard, a SQUID magnetometer made by SHE, and subsequently the flip coil, I nulled the ambient field in the region of the chip mount block to below $1\phi_0$ This

nulling centered on a position in the shields believed to be the final chip position. When the initial experiments finally began, the sense coil and chip positions had changed slightly, although I don't expect they were located in an ambient field of significant magnitude (that is, greater than $10\phi_0$ over the chip area).

Yet, upon trying to loosely correlate the ambient field with the number and orientation of flux quanta in a single row on a chip, I did not achieve satisfactory results. Instead I found that the number and orientation of flux quanta in a single row only marginally corresponded to the ambient field applied with the field generation coil. Take for instance the following plot (Figure 22) consisting of four scans across a single row. Each scan represents a separate flux trapping trial. The first had a $32\mu G$ positively applied field. $32\mu G$ is enough to populate half the holes on the entire chip. (This assumes that only flux within the perimeter of the hole array becomes trapped. All flux vortices generated on the border of the chip at $T_c$ travel to the edge and dissappear into a general "Meissner Effect" around the chip.) The second scan had a $32\mu G$ negatively applied field. The third and fourth scans had $64\mu G$ applied negatively and positively respectively.

Upon examining this plot, one can conclude that the flux vortices did move around with successive reheating of the chip. But the number of vortices present do not correlate to the magnitude of the applied field. Out of 8 holes in a row, only one or two are occupied. I did typically observe, however, that upon raising the ambient field, the orientation of the vortices would obey the direction of the applied field. This is evident here in the case of the third and fourth trials.

In light of what we know about thermally generated circulating currents, and our results with the flux scanner, it seems reasonable to postulate that the flux scanner fell victim to these thermal currents. S. Bermon has observed the effects of field-producing thermal currents in flux-trapping chips which he attributes to his conductive chip holder[3] When heating a chip, his chip holder would consistently generate a field on the order of forty microgauss. Because

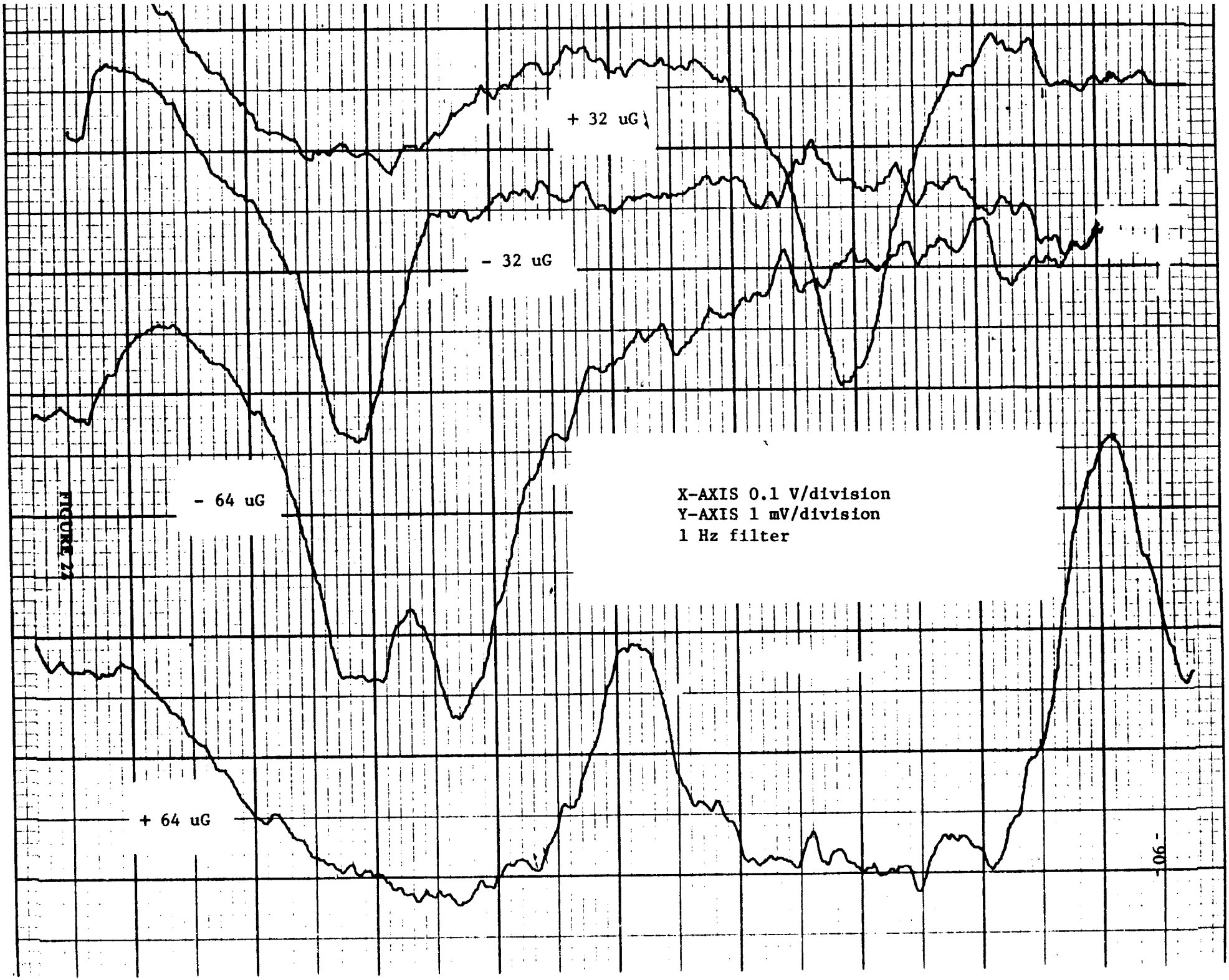
+ 32 uG
- 32 uG
- 64 uG
+ 64 uG
X-AXIS 0.1 V/division
Y-AXIS 1 mV/division
1 Hz filter
FIGURE 22
-90-

of the massiveness of the flux scanner apparatus, in close proximity to the heater and the chip, these effects are probably magnified. It is not unreasonable to expect that thermally generated fields on the order of tens of microgauss may be produced with the present method of heating.

Thermal currents generally arise from a temperature gradient along the interface between two dissimilar metals in contact. The temperature gradient produces a voltage gradient along the two metal junction which in turn generates a measurable current. We avoided using dissimilar metals in close proximity to the chip position for precisely this reason. Within 7" of the chip, aluminum is the only conducting metal present. However, aluminum is not perfectly isotropic. For this reason, thermally generated currents still exist, although to a lesser degree than if we had dissimilar metals present [4].

There are several possible steps one could take to ameliorate the situation. One is to more slowly heat and cool the chip. It is presumed that rapid cooling enhances sharper thermal gradients, and thus, larger amounts of stray flux. Another step would be to use insulating materials for the larger metal pieces in the lower part of the flux scanner. We originally ruled this idea out because of the dearth of insulating materials with a coefficient of contraction similar to Al. However this still may be feasible. Thirdly, a different, more uniform heating and cooling method could be used, which involves controlling He exchange gas pressure in a double-wall vacuum housing surrounding the apparatus. At any rate, for the flux scanner to be useful in data gathering experiments, one has to be able to control the number of flux quanta trapped in a single trial. I believe that with some further investigation, this can be accomplished.

## NOTES

1. J. Clem and S. Bermon, IBM internal presentation entitled "Theory of Flux Trapping in Perforated Superconducting Thin Films", (1982)

2. S. Bermon and T. Gheewala, Moat-Guarded Josephson Squids, Presented at the Applied Superconductivity Conference, (1982)

3. S. Bermon, private communication

4. S. Bermon, private communication

# CHAPTER V: CONCLUSION

## SUMMARY

The basic objective of the flux scanner experiment has been accomplished. A device has been developed which can detect single flux vortices trapped in a superconducting thin film. The highlights of this device fall into four categories:

First is the mechanical assembly. The MA moves a flux-detecting probe within a 0.375 inch square area while maintaining a separation distance of .0017 to .0023 inches between the probe and thin film. The design of this chip-scanning apparatus required a considerable effort due to the fact that it has to be operable at $4.2\,^{\circ}K$, and that it had to be built with custom non-magnetic parts. Some of the difficulties we faced in this respect were: thermal contraction of materials, water vapor evacuation, non-uniform cooling, thermal conduction between the helium bath and the outside environment, small diameter dewar necks, remote motor control, and remanent magnetization of materials.

The second part of the flux scanner is the flux detection system which consists of a SQUID magnetometer and a sense-coil. Most important to resolving individual vortices in a film was the sense-coil design. The design we used pushed the minimum physical size of hand-wound solenoids to the limit. Using the smallest gauge superconducting wire available (.002 inch diameter), we wrapped 9 turns in two layers on an absolutely minimal .009 inch diameter. The length of the solenoid and number of windings were optimized for maximum flux transfer from a trapped vortex to the input loop of our rf-SQUID. With our final design, we achieved a planar resolution of 0.015 inches, with the peak signal-to-noise of a typical vortex trace being 5 to 1.

The third part of the flux scanner is the magnetic field control apparatus. This consists of two ferromagnetic shields, nulling coils in all three dimensions, and a rotatable field generation coil. The objective was to reduce the absolute field in the chip position to a value, below which, not one flux vortex would be generated in the thin-film upon cooling through $T_c$. Since our shields could not do this alone, we used a coil in each dimension to assist in reducing the ambient field. Because the coils generate a uniform field across the chip, we anticipated that we could easily null the absolute field below the critical flux trapping value. But we were not assured that the field gradients inside the shields would be less than the critical flux trapping value per chip width. So we tried to orient the flux scanner in a position where the gradients would be smallest. It turned out that this shielding scheme was adequate for our purposes of testing the flux scanner's operation. We estimated the critical flux trapping value to be 1 $\mu$G. After nulling, the absolute field in the center of the chip was on the order of several micro-gauss. The field gradients over the 1/4" chip width were only slightly greater. (In the vertical direction the gradient of the field perpendicular to the chip was 1.5$\mu$G/quarter inch, and in the horizontal direction it was 2.25$\mu$G/quarter inch.)

The fourth and final part of the flux scanner device is the analog/digital electronic motor control unit. This part will facilitate experiments which require gathering large amounts of raw data. It will automatically scan a chip, line by line, recording on an X-Y Plotter the flux distribution across the chip. The output resembles a three-dimensional contour map. This electronic unit controls the two low-noise DC motors which move the probe over a chip. It also reads the two feedback potentiometers which record the current probe position. The precision of the motor movement exceeds the resolution of the sense-coil, ($\cong$ .002 inches), so it in no way limits the operability of the flux scanner.

Together, these four major component pieces of the flux scanner make it a viable scientific instrument. In its present state, it can be used for limited observations of vortices in various thin-film structures. With additional improvements to each of the four parts described

above, (to be discussed in the following section), the reliability and performance will be certainly increased to the degree that repeated automatic scans of a chip in a finely controlled field will be possible.

Hence, this thesis accomplished its major goal of demonstrating that individual vortices can be observed in their trapped position on a chip. Beyond that, it provided the groundwork for use of the flux scanner as a bonafide experimental tool. Its contributed to the understanding of how to construct such a tool, and how to ensure its reliable operation. Several significant problems were faced and solved. None of the remaining uncertainties concerning the operation of the device appear to be unsolvable. I have confidence that, with several more months of concerted effort, it can and will be used for regular experimentation.

## FUTURE IMPROVEMENTS

Fortunately, at the point I ran out of time to work on the flux scanner, the device's basic operability had been demonstrated and the major difficulties with its operation were understood. Now, the next step is to further investigate these difficulties and then fix them. The three basic problems I encountered were: arbitrariness in the horizontal positioning of the chip over the sense-coil, inability to correlate the field generated by the rotatable saddle-coil with the number of flux quanta trapped in a chip, and finally, delayed noise in the SQUID response when repositioning the sense-coil over a chip. Because the sources of these problems are understood, I forsee they are solvable. The following three sections elaborate further upon each problem in detail. There is also a fourth section which discusses a less immediate concern. This is an improvement to the flux-detection apparatus, specifically the sense-coil and transformer.

### Double Slide Assembly

During automatic chip scans, I had the difficulty that for the first few vertical sweeps, the horizontal chip position would not change. This happened even though horizontal stepping pulses were applied at the end of each vertical sweep. The problem was that the slider inside the horizontal slide assembly could twist slightly inside its track. Since the probe-arm attaches to the slider at one end, and extends 7.5 inches down to the chip, a small rotational displacement at the slider position results in a large displacement of the chip. This causes the chip to remain in the same horizontal position over the probe until the rotational slack is taken up and the slider can't twist any further. Basically, this is a backlash problem. Whenever the horizontal movement of the probe arm is reversed, the chip end of the probe arm remains stationary for a short while until the motor twists the slider as far as it will go. Then the chip will begin to move over the probe. This problem is exacerbated by the fact that a significant

frictional force from the teflon glides holds the chip end of the probe arm encouraging the slider to twist inside its track.

The side-effects of this problem are that the chip moves on a slight diagonal over the probe. In other words, the sweeping direction of the chip is not quite parallel to the rows in the hole array on the chip. This degrades the readability of the output plots because the signal from vortices trapped in a row is not uniform. To solve these problems, I redesigned the lower mechanical assembly of the flux scanner. It now employs two slide assemblies-- one is 7" above the chip position, and the other is 7" below the chip position. The probe arm now attaches at both ends, each end being connnected to a slide assembly. This removes the probe-arm twist, and generally improves the horizontal chip positioning with respect to the probe.

**Heater Redesign**

As mentioned in Chapter IV, when attempting multiple flux trapping trials in a single chip, the number of flux quanta trapped did not correlate with the applied field. I postulated that this was at least partly due to thermally generated currents circulating in the flux scanner assembly during heating and re-cooling of the chip. Based on results from other experiments, it is not unreasonable to expect such fields to be in the 10-100 $\mu G$ range, which is on the order of the applied fields [1]

To solve this problem, it is thought that reducing thermal gradients in the vicinity of the chip will diminish the circulating currents around the chip. Since the glass-walled evacuation tube is in contact with the helium bath, a severe temperature drop presently exists from the tube to the heater. If a vacuum-tight double-wall glass tube was constructed, one could control these temperature gradients during cooling by the amount of exchange gas between the two walls. The exchange gas pressure would determine the cooling rate of the inner wall, and thus, would control the temperature gradients inside the inner wall.

WIth a double-wall tube, the procedure for heating a chip would be as follows. The exchange gas within the walls, which keeps the flux scanner at 4.2 $^{\circ}K$, would first be pumped out. Then heat would be applied to the chip so that it warmed up. Finally, the heater would be turned off, and exchange gas would be slowly leaked into the evacuated region. The flux scanner apparatus would hopefully cool without producing any thermal emfs. Then we could determine whether correlation of the applied field with the amount of trapped flux is possible.

**Thermal Isolation of the SQUID**

During actual flux scanner measurements on the 8×8 array of flux attractive holes, I observed that after halting the motors, the SQUID response would continue to rise. It is highly unlikely that this effect was induced by a suddenly changing external field, especially since it recurrently happened after moving the sense-coil as short distance. After paying closer attention to this phenomenon, I also regularly noticed that the SQUID response would steadily drop at the beginning of a trace. This happened even though no flux change through the sense-coil was expected in that area. Finally, I observed upon heating a chip, that the SQUID response would fall as the chip heated, and than rise again as the chip was cooled [2] For these reasons it appeared conclusive that the mechanical movement of the flux scanner slide assembly generated heat which affected the SQUID.

The most straightforward solution to this problem is to thermally isolate the SQUID from the mechanical scanning apparatus. This can be accomplished by thermally anchoring the SQUID to the liquid He bath. Using beryllium-copper fingers, one could make sure the SQUID contacted the glass evacuation tube at a point where it was immersed in the bath. Eliminating this dependence of the SQUID response on the mechanical probe arm movement would certainly improve the quality of the plots from automated scans. All extraneous temperature-induced effects would be muffled which would improve the plots' readability.

**Thin Film Sense-Coil and Transformer**

Improving the resolution of the sense-coil would allow examination of smaller hole structures etched through thin films. In fact, one might even be able to look at trapped flux in Josephson circuit chips. One method to achieve this finer resolution would involve fabricating a thin film sense-coil and transformer [3] Since a multi-turned sense-coil of that size would have an inductance on the order of picohenries, a transformer would be necessary to improve the flux transfer between the sense-coil and SQUID input loop. The major difficulty with this scheme is fabricating superconducting contacts to the chip. At the present time, there is no established technology for bonding superconducting leads to superconducting pads on a chip. If this problem can be easily solved, the possibility of an increased scanning resolution is substantial.

## NOTES

1. S. Bermon and T. Gheewala, Moat-Guarded Josephson SQUIDS, Presented at the Applied Superconductivity Conference, (1982).

2. Actually, this effect was only noticeable for small temperature changes. For larger fluctuations, the SQUID response was oscillatory. It appeared as though heating the SQUID shifted the operating point on its intrinsic interference pattern.

3. M. B. Ketchen, IEEE Trans. Magn., **MAG-17**, (1981).